OULUN YLIOPISTO
University of Oulu

DEGREE PROGRAMME IN ELECTRICAL ENGINEERING

MASTER'S THESIS

BEHAVIOR OF THE RF POWER AMPLIFIER UNDER A VARYING LOAD CONDITION IN 5G MASSIVE MIMO BASE STATION

Author	Anssi Karhu
Supervisor	Timo Rahkonen
Second Examiner	Janne Aikio
Technical advisor	Mikko Nieminen

August 2018

Karhu A. (2018) Behavior of the RF Power Amplifier Under a Varying Load Condition in 5G Massive MIMO Base Station. University of Oulu, Department of Electrical and Information Engineering. Master's Thesis, 68 p.

ABSTRACT

RF power amplifier is located at the backend of the transmitter before the filter and the antenna. To ensure ideal operation, known output impedance of the power amplifier is matched to the load impedance with help of matching network. Load impedance is traditionally provided by the circulator which has good isolation properties and stable load property.

Higher frequencies are investigated in the future 5G technology to obtain wider available bandwidths and meet increased capacity requirements. Higher frequencies have shorter wavelength which leads to smaller cell sizes due to their poorer propagation capability. As many RF components, also antennas have properties that are relative to wavelength. Higher frequency thus enables to integrate more antenna elements to base station structure, which is called massive MIMO (mMIMO) structure. By adjusting excitation signals of each element, wanted beam forms and beam directions are achieved.

The possibility for the removal of the circulator from the power amplifier output was investigated in this thesis. In mMIMO structure number of transmitting branches is huge, so there is potential to achieve cost savings and increase the integration level if the removal is feasible. However, transistor output would be then altered to highly frequency and power dependent load, because the antenna input impedance is affected by the coupling effects from neighboring elements as a function of beam steering functionality. Thanks to good isolation properties of the circulator, power amplifier is not altered to that in traditional base station design. Additionally, circulator protects the transistor from reflecting waves, as they are routed to the termination.

The device under test was optimized to 3.4 GHz-3.6 GHz frequency band and was connected as a balanced structure. The goal in this thesis was to investigate how the removal is changing the behavior of the power amplifier compared to the design where the circulator exists. Investigation was carried out by examining the basic RF performance parameters and quality of the feedback response for the digital pre-distorter (DPD). Simulation models turned out to be inadequate to simulate the performance under a varying load condition properly and accurate correlation between simulations and hardware measurements was not achieved. However, hardware implementation and measurement results showed up a potential, but there also occurred a big variation over the operation bandwidth. There occurred 8.3% unit variation in the efficiency figures in the circulatorless design over the bandwidth while it was just 2% units in the design where circulator existed. Peak power quantities varied 1.5 dB and. 0.5 dB respectively. Also, the effect on the DPD feedback response was more severe than expected as the ripple in the response was 4 dB in the circulatorless design while it was within acceptable limits in the design where the circulator existed. Therefore, more investigation would be needed in the future to ensure the proper performance over the bandwidth.

Key words: circulator, coupling effect, antenna element, beam forming

Karhu A. (2018) RF Tehovahvistimen käyttäytyminen vaihtelevan kuormaolosuhteen alaisuudessa 5G massive MIMO tukiasemarakenteessa. Oulun yliopisto, sähkö- ja tietotekniikan osasto. Diplomityö, 68 s.

TIIVISTELMÄ

Tehovahvistin sijaitsee tukiasemarakenteen lähetysketjun loppupäässä ennen suodatinta ja antennia, ja on tukiaseman eniten tehoa kuluttava osa. Jotta tehovahvistin toimisi ideaalisesti, sen tiedetty lähtöimpedanssi sovitetaan sovitusverkon välityksellä kuormaimpedanssiin, joka perinteisesti on hyvän isolaatiokyvyn omaavan sirkulaattorin tuottama kuorma.

Tulevaisuuden 5G-teknologiassa signaalitaajuus tulee useimmissa tapauksissa kasvamaan, sillä vapaata taajuuskaistaa ei juurikaan ole enää saatavilla nykyisillä langattoman tiedonsiirron käyttöön osoitetuilla taajuusalueilla. Tätä lisäkapasiteettia on välttämätöntä saada, jotta huimasti kasvavaan langattoman tiedonsiirron tarpeeseen kyetään vastaamaan. Korkeammat taajuudet tarkoittavat lyhyempiä aallonpituuksia, joiden myötä signaalin etenemiskyky heikkenee ja tukiasemien solukoot pienenevät väistämättä. Kuten RF-komponentit usein, myös antennielementit omaavat useita aallonpituudesta riippuvia parametreja. Täten taajuuden kasvattaminen sallii myös antennielementtien määrän kasvattamisen, jolloin puhutaan Massive MIMO (mMIMO) rakenteessa. Näiden antennielementtien välisiä konfiguraatioita muuttamalla saadaan aikaan haluttuja keilakuvioita ja kyetään myös suuntaamaan keiloja haluttuun suuntaan. Tätä kutsutaan keilanmuodostukseksi (engl. beamforming).

Tässä työssä tutkittiin päätesirkulaattorin poistamisen mahdollisuutta tehovahvistimen lähdöstä 5G mMIMO -tukiasemarakenteessa. Lähetysketjujen suuresta määrästä johtuen integrointitason kasvattaminen omaa suuren potentiaalin kustannussäästöihin, ja sirkulaattorin poistaminen varsin isokokoisena ja hintavana komponenttina olisi myös yksi vaihtoehto niiden saavuttamiseksi. Tällöin tehovahvistimen näkemä kuorma on kuitenkin taajuuden ja tehon funktiona vaihteleva, sillä antennin tuloimpedanssiin vaikuttaa esimerkiksi kytkeytymisefektit viereisistä antennielementeistä eri keilanmuodostus konfiguraatioiden funktiona. Perinteisessä toteutuksessa sirkulaattori siis stabiloi hyvän isolaatio-ominaisuutensa ansiosta tätä vaihtelevaa kuormaa tehovahvistimen näkökulmasta, sekä myös suojaa tehovahvistinta takaisin heijastuvilta aalloilta.

Työ toteutettiin tutkimalla, miten sirkulaattorin poisto vaikuttaa tehovahvistimen toimintaan verrattuna toteutukseen jossa sirkulaattori on olemassa. Tutkittava integroitu Doherty vahvistin oli optimoitu taajuusalueelle 3,4–3,6 GHz ja oli kytketty balansoiduksi rakenteeksi. Työssä käytetyt simulointimallit osoittautuivat liian vajavaisiksi, joten tehovahvistimen suorituskykyä ei pystytty täysin mallintamaan. Käytännön mittaukset osoittivat kuitenkin potentiaalia, mutta myös suurta suorituskykyvaihtelua taajuuskaistan yli. Hyötysuhdeluvut vaihtelivat 8,3% yksikköä ja piikkiteho kyvykkyys 1,5 dB taajuuskaistan yli toteutuksessa jossa sirkulaattori oli poistettu vastaavien lukujen ollessa 2% yksikköä ja 0,5 dB toteutuksessa jossa sirkulaattori oli olemassa. Lisää kehitys- ja tutkimustyötä tarvittaisi, jotta tehovahvistimen käyttäytyminen saataisi varmistettua koko taajuuskaistan ylitse.

Avainsanat: sirkulaattori, kytkeytyminen, antennielementti, keilanmuodostus

TABLE OF CONTENTS

FOREWORD

This Master's thesis was carried out in Nokia Oulu, and the purpose was to investigate the possibility for circulator removal from the power amplifier structure in the future 5G mMIMO TDD base station.

I am very grateful to my former line manager Jari Myllylä who hired me as a summer trainee couple years ago the very first time. And what a journey it has been so far. I would like to thank the whole power amplifier R&D team for a great support throughout my thesis work and for being such a fun team to work with. I would like to give my special thanks to Mikko Nieminen for being technical advisor and close support for my thesis. Also thanks to my line manager Janne Soppela for giving me time to finalize my thesis. Special mention to Satu Harvala and Teppo Utterström of many good late evening discussions at the office.

I express my gratitude to Prof. Timo Rahkonen for supervising this thesis with his expertise. I also thank Dr. Janne Aikio for being a second examiner.

Another special mention for my fantastic fellow students. Together we have battled through many difficult tasks, working late and have had such a fun time outside the university as well. Good times.

I want to thank my parents for supporting me all my life. Thank you, my fantastic brother Atte, for always being you. Never change.

Last but not the least, I want to thank all my long-time friends for giving such a lot joy to my life. I really appreciate it.

Oulu, August 13. 2018

Anssi Karhu

LIST OF ABBREVIATIONS AND SYMBOLS

5G	5th generation
AM-AM	Amplitude to Amplitude Conversion
AM-PM	Amplitude to Phase Conversion
CS	Common Source
CW	Continuous Wave
DAPD	Digital Adaptive Pre-Distortion
dBm	Decibel relative to one milliwatt power
FDD	Frequency Division Duplex
GaAs	Gallium Arsenide
GaN	Gallium Nitride
IM	Intermodulation Distortion Product
IoT	Internet of Things
LDMOS	Laterally Diffused Metal Oxide Silicon
LTE	Long Term Evolution
MIMO	Multiple Input Multiple Output
mMIMO	Massive MIMO
MMIC	Microwave Monolithic Integrated Circuit
mmW	Millimeter Wave
PAE	Power Added Efficiency
PAR	Peak to Average Ratio
PCB	Printed Circuit Board
RF	Radio Frequency
RX	Receiver
Si	Silicon
SISO	Single Input Single Output
TDD	Time Division Duplex
TPF	Temperature Power Feedback
TX	Transmitter

$\Delta\varphi$	*Phase shift between two successive antenna elements*
A	*Signal Amplitude*
B	*Channel Bandwidth*
C	*Theoretical maximum bit rate*
D	*Distance between transmitter and receiver*
d	*Distance between radiating elements*
f	*Signal Frequency*
G	*Power Amplifier Gain*
G_A	*Antenna Gain*
K	*Voltage Gain*
k	*Power series coefficient*
N	*Number of antenna elements in the array*
P_{RF}	*Output power from the Power Amplifier*
P_T	*Transmitted Power*
P_R	*Received Power*
S/N	*Signal to noise ratio SNR*
V	*Voltage*

ω	Angular Frequency
η	Power Amplifier drain efficiency
λ	Lambda, Signal wavelength
θ	Theta, Beam steering angle

1. INTRODUCTION

Future 5G wireless communication technology seems to be coming faster to the markets than anyone could have imagined. Development has been fast and first proof of concept demo networks have been built already. Operators have accelerated their schedules practically by a year from the initial plans, and 5G implementation seems to take place in 2019 instead of 2020. Industry is thus being forced to do enormous work to accomplish the market needs. Integration level increases, productization gets faster and electronics design gets more complex.

In many discussions, 5G often refers automatically to extremely high frequencies, millimeter wave (mmW) frequencies, but 5G technology will not replace the existing microwave frequencies entirely. Most likely they are both employed in 5G architecture, where microwave frequencies are utilized for long-range outdoor communications and mmW frequencies are more suitable for high data rate communications in areas where more capacity is needed. The migration to higher frequencies is done in hope for wider available bandwidths, but availability in sub 1 GHz frequency ranges are explored in certain areas too.

Due to naturally poorer propagation capabilities of higher frequencies, cell sizes will be smaller in the future, and transmitting power can be decreased in each transmitter (TX) branch. Additionally, higher frequency enables to pack more antenna elements into an array and the base station coverage performance is therefore carried out more via antenna array functionalities in the future. This multiple input multiple output system where even hundreds of antenna elements are existing is called Massive MIMO (mMIMO). To increase base station functionalities and meet mMIMO requirements, also powerful software is required. However, no considerations are taken there, as this master thesis work is hardware R&D related.

As the amount of TX/RX branches is increased in the future 5G mMIMO technology, it requires internal hardware implementations to be also more cost and space effective. First proof of concept demos and client products are possible to be carried out partly based on old hardware solutions but latest when the 5G technology matures, also internal hardware structures are needed to be more innovative in addition to new general level solutions.

The power amplifier (PA) block is thus under evaluation too and one possibility in the power amplifier block level could be the removal of output circulator to fulfill the pressure of increased cost and size requirements. The goal of this thesis was to understand the background of the mMIMO structure better and deepen the co-operation between cross-functional teams. General level understanding was needed, as the removal of circulator alters power amplifier to highly changing load property provided by the combination of filter and antenna. The goal was not to adapt to changing load properties, but to explore if the RF performance still remains within acceptable limits even though the circulator removal leads to load instabilities and higher-level reflections.

Strong base theory is first presented because thesis is not just power amplifier related, but requires understanding also from the antenna behavior. Base theory is followed by the simulation work that included large signal simulation for finding the load properties used later in hardware measurements. RF performance was simulated with a load-pull data based model and the design was then verified with hardware implementation.

2. WIRELESS COMMUNICATION

When taking a glance to history, it is noticed that the wireless communication systems have undergone a revolution approximately every ten years and development has been massive from 2G GSM systems presented in 90s via 3G WCDMA systems until todays 4G LTE wireless networks. Again, as the 2020 is approaching, new generation is under development to fulfill the increasing demand for the high speed and sensitive data traffic.

The development and discussion regarding the forthcoming fifth generation 5G network has been led by industrial needs, machine to machine, Internet of Things (IoT) and high data rate communications systems (Gigabits per second) that require low latency ("zero latency") and support for large number of simultaneous users (10-100 times the number of connected devices in 4G). The evolution to 5G technology enables a wide scale of new use cases transforming industrial processes and enriching leisure time activities by digitalizing event experiences and providing capability to transmit extremely high-quality streaming services wirelessly. [1][2]

It is expected that active mobile broadband subscriptions are increasing massively due to fact that 5G wireless communication involves not only humans but practically all devices that have any kind of functionality. The total amount of mobile broadband subscriptions is increasing worldwide at about 20 percent a year on year pace, and it is anticipated that 4G LTE technology bypasses the 3G as a dominant mobile access technology by the end of 2017. It is also forecasted that only 5G subscriptions themselves are increasing from zero to amount of 1 billion by the end of 2023 while there are then approximately 8.5 billion mobile broadband subscriptions in total including 3G, 4G and 5G. [3]

However, not only number of mobile broadband subscriptions are going to increase but also the mobile data traffic is increasing enormously year by year. The data traffic is expected to be by total amount of approximately 8 times larger in 2023 compared to 2017. This is mainly fueled by seamless connectivity of society where more viewing of high quality video content and using other innovative services with connected devices takes place. [3][4]

2.1. Wireless communication spectrum

To meet the increasing data rate and capacity requirements, higher spectrum bandwidths are needed and they will be introduced in fifth generation technology. The theory for the channel capacity is known as Shannon theorem (1), which shows that improvement in bandwidth or signal to noise ratio SNR enables higher data rate.

$$C = B \log_2 \left(1 + \frac{S}{N}\right), \tag{1}$$

where

C is the theoretical maximum bit rate [b/s],
B is the channel bandwidth [Hz] and
S/N is the signal to noise ratio, SNR.

This is the reason for migrating towards higher frequencies. Today's mobile telecommunications spectrum is mainly located below 3 GHz where free spectrum has become scarce resource in traditional frequency bands assigned for the mobile telecommunications. Certain amount of frequency band is allocated for operators and therefore limited bandwidth is available for each. Signals with 20MHz carrier bandwidths are maximum in today's 4G technology whereas several hundreds of MHz carrier bandwidth signals are aimed to use in the future 5G technology. These wider bandwidths are most likely to be found from higher millimeter wave (mmW) frequencies which are considered to be higher than 30 GHz. [1]

Even though the available bandwidth may be large in mmW frequencies, the propagation characteristics of such high frequency signals differ a lot from the ones that are located at today's microwave frequency bands. The migration to higher frequencies leads to increased point-to-point propagation path losses in the communication channel due to lower wavelength of the signal. This can be seen from Friis equation (2) where D is the distance between transmitter and receiver in meters and P_R and P_T are received power and transmitted power, respectively. The equation results to fact that the path loss grows with the square of the carrier frequency in case antennas with the unity antenna gain, $G_T = G_R = 1$ (isotropic antennas), are used.[5]

$$\frac{P_R}{P_T} = G_T G_R \left(\frac{\lambda}{4\pi D}\right)^2 \tag{2}$$

Different kind of fading and scattering properties also get more complex. Leafage loss caused by the trees obstructing the signal gets much increased, rain attenuates the signal more and mmW signals are influenced by the effect of diffraction and shadowing much greater than microwave signals. For instance, compared to microwave signals, high frequency signals observe higher blockage losses in bricks, concretes and human body.[6]

Despite current mobile cellular spectrums, located below 3 GHz, are becoming congested during busy hours in highly loaded cells, these sub 6 GHz frequencies are also considered to deploy 5G technology alongside with the higher mmW frequencies. Both are needed: sub 6 GHz frequencies for providing wider coverage with reasonable capacity while high frequencies are needed to meet ultra-high broadband speeds. Several suitable frequency bands are considered where 3.3-3.8 GHz band is expected to form the basis for 5G deployment and above 30 GHz frequencies are being investigated due to their natural availability for wider spectrum resources as they are absent from today's mobile telecommunication spectrum.[7]

2.2. Base station

Up to the latest 4th generation technology, base stations have traditionally been Single Input-Single Output (SISO) structures where high-power RF signal is radiated via one antenna element. Due to high transmit power together with lower carrier frequency (larger wavelength) the cell size has been large. This is a remnant of the very first wireless communication generations, where the large coverage was always aimed. Alongside the 5G technology, 4G LTE technology will still be further developed. The goal is to get the most out from the existing technology too by focusing on optimizing

the spectral efficiency in existing frequency bands and using advanced functionalities such as carrier aggregation and Multiple Input-Multiple Output (MIMO) structures. This so-called LTE-Advanced technology allows to use 4x4 MIMO structure where multipath propagation can be good used by combining the signal from multiple antenna systems because the signal path corresponding to different transmit-receive pairs experience different propagation losses. Another technique for achieving wider bandwidths, in addition to totally new frequency bands, is carrier aggregation. Carrier aggregation sums maximum bandwidths from several LTE frequency bands and as a result up to 100 MHz total bandwidth can be achieved thus enabling higher peak data rates.[4]

The role of the power amplifier (PA) in the base station structure and the foundation for the simultaneous two-way communication, duplexing, is introduced in the following chapters.

2.2.1. Two-way communication

In wireless communication systems two-way communication is essential. For that purpose, duplex communication is needed where transmitting and receiving can take place simultaneously.

There are two methods available for separating the downlink and uplink communication, time division duplex (TDD) and frequency division duplex (FDD), which are introduced in Figure 1. Frequency division duplex separates TX (downlink) and RX (uplink) communication based on different frequency bands. In TDD technique the separation between transmission and receiving is carried out by periodically allowing either downlink or uplink communication. Perhaps the biggest advantage is that the total bandwidth is thus allocated to use and spectral efficiency is high but, on the other hand, there is guard time needed between uplink and downlink communication which increases the latency. Time division duplex is the most used duplexing technique in fourth generation broadband systems and will also be in a key role in future fifth generation base stations and smart antenna MIMO structures. [8]

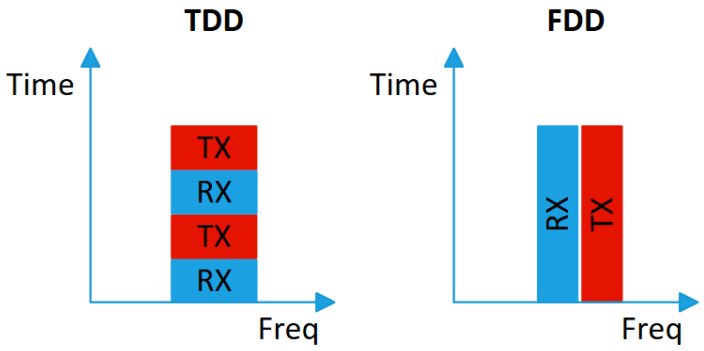

Figure 1 Difference between TDD and FDD system in terms of separating the uplink and downlink communication.

2.2.2. Power amplifier in the base station structure

Power amplifier (PA) is located at the backend section of the base station. The purpose of the power amplifier is to amplify the low-level radio frequency (RF) signal to an appropriate level for transmitting it to user equipment (thousands of time higher from input to output). Multi-staged amplifier structure is generally utilized to provide high enough gain to amplify the input RF signal to the sufficient output power level. Power amplifier must be able to fulfill output power requirements that typically are even 40 – 100 W nominal RMS output power with substantially higher peak power capability in traditional large cell applications. The block diagram of the base station backend section and how the PA is located within the transmitting (TX) chain can be seen in Figure 2. Power amplifier is followed by a bandpass filter which removes the harmonic frequencies before transmitting amplified RF signal via the antenna element. [9]

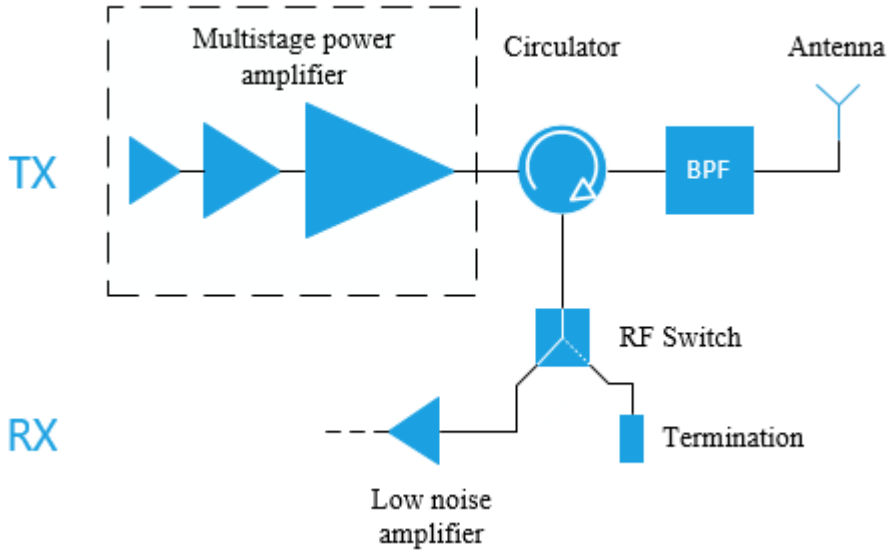

Figure 2 Block diagram of the TDD base station backend structure.

Antenna is reciprocal which means that the same antenna both transmits and receives the RF signal. The separation between the receiving (RX) and TX chain is implemented with duplex filter in FDD system while the TDD radio uses switches. There is traditionally circulator placed to the output of the power amplifier to route the RX into different path than TX signal in TDD structure. It is then followed by the RF switch to either route the signal path to termination during the transmitting or to the LNA during the receiving. In the FDD structure, the isolator handles this protection functionality against reflections similarly during the transmitting. The circulator thus protects the PA against reflective high-power signals during transmitting in case there are any unmatched loads that causes the high power leveled reflections. The other reason for using the circulator is to provide a stable load for the PA output and thus enable the better power match and therefore better power delivery towards the antenna. There are many requirements that are needed to keep in mind when designing a RF power amplifier and they will be discussed in chapter 4.

3. 5G MASSIVE MIMO BASE STATION

Large cells alone are not anymore suitable for future high data transfer communications where maximum number of users are needed to be served with an ultimately high performance, instead of aiming for large coverage only. Cell sizes are getting smaller and the same coverage which is achieved with one base station in previous generations will be now dealt with multiple high functionality base stations. Network coverage performance, capacity and energy efficiency can be enhanced through this network densification. [6]

As presented in the section 2.1 “Wireless communication spectrum”, higher frequencies have attracted significant interest to obtain larger available bandwidths (hundreds of MHz). When higher frequencies are used, the network densification towards smaller cell sizes kind of takes place naturally too due to their poorer propagation capability. To overcome the drawback with their natural poor propagation capability presented in the section 2.1, there is a necessity to find alternative solutions in a base station perspective as well.

Even though the higher frequency (lower wavelength) leads to higher propagation losses and blockage effects, it also consequently enables designers to pack more antenna elements into the same effective area. This is because the optimum sizing for the antenna radiator and element spacing is wavelength dependent and is generally sized to $\lambda/2$. The implementation where multiple antenna elements are summed together is called antenna array, which is key to MIMO structure. Compared to latest evolution of 4^{th} generation technology, where maximum four or eight antenna elements are being employed, even 256 antenna elements are employable in the future 5G massive MIMO (mMIMO) base stations. This is also the difference behind these two nominations. [6]

Massive MIMO structure is becoming a promising proposition to be deployed in 5G technology where transmitting takes place with a much lower power due to smaller antenna size in higher mmW frequencies. So, to generate even small coverage, efficient and developed antenna solutions are needed to be implemented as well. Massive MIMO 5G base stations have many highly specific functionalities such as antenna beam steering, where the antenna beam can be controlled to highly loaded areas and service capability can thus be dynamically changed. In addition, there is capability to serve hundreds of users in the same time-frequency resource, or produce multi-user property by allocating different RF frequency transmit paths to take place via several individual antenna sub arrays. [6]

3.1. Power amplifier in the 5G mMIMO base station

Due to smaller power handling capability of mmW antennas and smaller cell sizes, also lower transmitting power is required in the future 5G technology. While the transmitting power is generally 40 W in traditional large cell applications, approximately 5-10 W in each TX branch is needed in mMIMO structure.

As the transmitting power will be decreased in 5G mMIMO base stations, also the nature of power amplifier stage will most likely change and it will be more about handling the entity. Due to lower wavelength and transmitting power, the overall size for electronics and matching networks gets smaller. This also enables transistor vendors to fit more into less and the power amplifier technology will be most likely

developing from today's individual amplifier stage with external matching circuits towards modules, which are 50 Ω in 50 Ω out designs where all the inter-stage matching and multistage amplification is performed "under the hood". It is vital to explore new solutions for the future cost efficient 5G mMIMO base stations where high level of integration is essential, and requirements for PA section properties, such as its cost and physical size, are under the investigation too. [10]

3.2. Antenna Array in the mMIMO structure

In mMIMO base station design perspective, power will be decreased in power amplifier stage but antenna gain can be increased. Antenna gain does not actually relate to amplifying the signal but thanks to antenna array structure, transmitting energy can be localized ("squeezed") to a narrower area to desired direction. Radiating power in mmW frequencies is small due to small antenna size hence requiring an efficient antenna array design to compensate lower transmit power. Antenna gain of single radiating element is relatively low and radiation pattern is relatively wide. By combining multiple elements together, higher directivity (gain) and configurable beam can be achieved and demand for longer distance communication can be accomplished. Total array gain can be expressed as

$$G_{Array}[dB] = 10 * \log_{10}(N_{Ant}) + G_{Element}[dB], \quad (3)$$

where

N is the number of antenna elements employed in the array and
$G_{Element}$ is the gain of each individual element.

Each antenna element employed in mMIMO structure usually has two radiators which are cross polarized to each other and both polarizations are excited with their own RF signal. By allocating elements differently, and exciting them individually, antenna beams can be controlled.

3.3. Antenna array properties and functionalities

In the 5G massive MIMO technology, thanks to large number of antenna elements, special functionalities are possible to be performed. Massive MIMO allows us to produce highly directional 3D antenna beam patterns by using analog, digital or hybrid beamforming. Sum beam direction and sidelobe properties can be steered by controlling the phase and amplitude coefficients applied to each single antenna element via the feed network. Sidelobe properties and the main beam beamwidth are adjusted by applying different amplitudes to certain elements and this is called tapering. By setting the phase shift between the two successive elements constant, beam steering angle for the combined beam is defined as

$$\theta = \sin^{-1}\left(\frac{\Delta\varphi * \lambda}{360° * d}\right), \quad (4)$$

where

Δφ is the phase shift between two successive elements,
d is the distance between radiating elements (i.e. λ/2),
λ is the wavelength and
θ is the beam steering angle.

As told earlier, adjacent antenna elements are generally λ/2 spaced to avoid the main beam of re-appearance on the wrong side of the reference plane. This so called grating lobe can occur in higher beam steering angles, and the capability decreases when the element spacing is increased. Beam steering functionality is presented in Figure 3. [6][11][10]

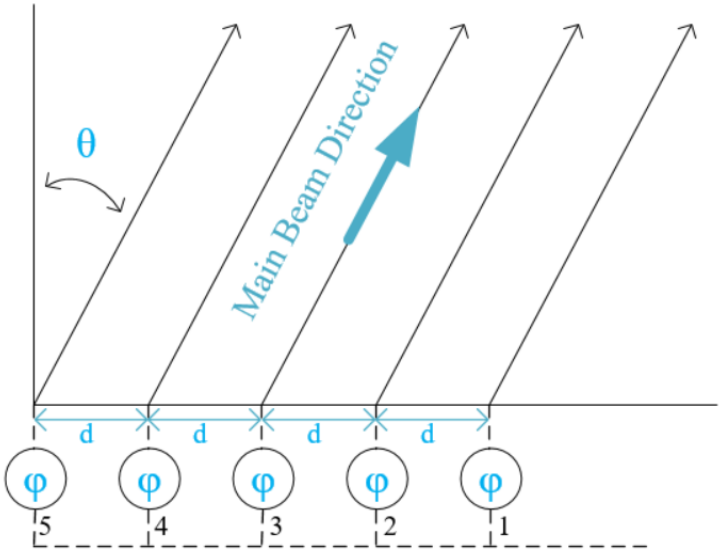

Figure 3 Beam steering functionality.

Individual mMIMO antenna element has not only frequency dependent but also excitation and phase steering dependent reflection coefficient in each TX branch, and it is also named as an active reflection coefficient. One of the important properties RF designer should be concerned about is the mutual coupling between the antenna elements in the antenna array. Part of the radiated electromagnetic energy from each element gets coupled to the surrounding elements thus effecting on the input impedance and radiation pattern properties of each individual antenna element. The element spacing and arrangement affect to the amount of coupling but in addition to that, antenna elements are experiencing dynamically changing environment where the beam steering angle and excitation level of neighboring elements influence too. Also, outer surroundings of an antenna can have significant impact on the impedance seen at the antenna input port. [11][12]

4. BASICS PROPERTIES OF POWER AMPLIFIER

Power amplifiers are characterized based on a few basic properties no matter whether they are intended to be use in traditional large cell applications or in the lower power small cell mMIMO applications. They work at relatively high-power levels in base station applications hence consuming a lot DC power which makes power efficiency an important property. Nonlinear behavior gives its limitations to whole base station performance and one should always make tradeoffs when tuning the PA towards the wanted performance. For example, if the aim is to achieve good linearity that makes the efficiency worse, higher peak power level worsens the linearity etc. So, to achieve good efficiency and acceptable linearity, linearization methods are usually needed. Basic PA properties and requirements are discussed in the following chapters.

4.1. Efficiency

Efficiency is generally defined as a relation of how the input resources are converted to effective output resources. Efficiency plays also a big role in the power amplifier design because currents are often very high when the base station is transmitting at the full power. The PA efficiency is also crucial in terms of total base station efficiency as the PA is a major power consumer in transmitter system. The dissipated power generates heat and therefore even a small fraction towards the better efficiency has a positive effect on the heat load and cooling requirements. This leads to smaller mechanics and physical size and better environmental values are also achieved. [13]

Most of DC input power is fed to transistor drain and therefore efficiency is usually defined as a drain efficiency. It means the relation between RF power delivered to load and DC input power. RF power is generally expressed as decibel referenced to milliwatt (dBm) which is then converted to watts when calculating the efficiency. The drain efficiency η is determined with equation 5

$$\eta = \frac{P_{RFO}}{P_{DC}}, \tag{5}$$

where

P_{RFO} is the gained output power from the amplifier and
P_{DC} is the consumed DC power at the transistor.

An alternative definition for defining the efficiency is called power added efficiency (PAE) where the input signal power level is also considered. From there it can be noticed that the smaller the power amplifier gain G is, the worse is the power added efficiency. With high gain levels drain efficiency η and PAE are approaching each other. PAE is defined as

$$PAE = \frac{P_{RFO} - P_{RFIN}}{P_{DC}}, \tag{6}$$

where

P_{RFIN} is the input RF power to power amplifier.

As already determined, power amplifiers usually consist of multiple stages. According to (7) the last stage gain and efficiency have the most critical effect on total power amplifier efficiency and therefore design of the last stage power transistor properties becomes essential. The total efficiency of the three-stage power amplifier can be calculated as

$$\eta_T = \frac{1}{\left(\frac{1}{\eta_1 G_2 G_3} + \frac{1}{\eta_2 G_3} + \frac{1}{\eta_3}\right)}, \tag{7}$$

where

η_n is the efficiency of each stage and
G_n is the gain of each stage.

From there it is also seen that in case the last stage gain is small, the better driver stage efficiency may then help. [14]

4.2. Linear power amplifier

An ideal power amplifier output quantity would be linearly proportional to the input quantity and the ratio between the output and the input is called the gain of the amplifier. The ideal amplifier produces a clear output response that does not have any additional frequency components within or outside of the amplifier bandwidth. The linear output response is determined with

$$V_{out}(t) = K_1 V_{in}(t), \tag{8}$$

where

$V_{out}(t)$ is the output voltage at the time,
K_1 is the voltage gain of the amplifier and
$V_{in}(t)$ is the input voltage at the time.

The ideal memoryless amplifier with a linear transfer characteristic is illustrated in Figure 4.

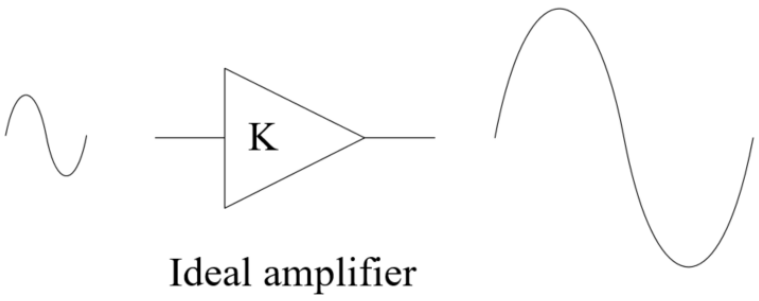

Figure 4 Ideal amplifier amplifies the input signal linearly.

4.3. Nonlinearities

There is not such an amplifier in practice that does not include any non-linear elements causing non-linear performance. Nonlinearity, and thus a real-life amplifier, can be modelled with an infinite power series

$$V_{out}(t) = k_0 + k_1 V_{in}(t) + k_2 V_{in}^2(t) + k_3 V_{in}^3(t) + \cdots K_n V_{in}^n(t), \quad (9)$$

where

k_0 is the DC-term,
$k_1 V_{in}(t)$ is the linear term and
$k_2 V_{in}^2(t), k_3 V_{in}^3(t), .. K_n V_{in}^n(t)$ are higher order nonlinear terms.

One set of power series coefficients k_n are constant for a fixed bias point and certain input and output impedances. Real value power series coefficients k_n model memoryless nonlinear system because the fundamental output is in phase with the input over the whole frequency range. Nonlinearities in the amplifier cause saturation and distortion and these nonlinearities are explained in following chapters. The existence of nonlinearities can be detected as either by generation of new spectral components or amplitude dependent gain and phase properties. [15][16]

4.3.1. Harmonic distortion

When the input signal amplitude increases, the amplifier is not able to amplify the signal linearly but begins to distort it by generating new spectral components. Distortion caused by a single tone signal is called harmonic distortion and the existence of the harmonic distortion can be evaluated when a sine wave signal

$$V_{in}(t) = A\cos \omega t \quad (10)$$

is applied to the input of the nonlinear power amplifier and thus replacing the V_{in} in (9). It gives

$$V_{out}(t) = k_0 + k_1 * (A\cos \omega t) + k_2 * (A\cos \omega t)^2 + k_3 * (A\cos \omega t)^3, \quad (11)$$

where

A is the signal amplitude,
t is time,
$\omega = 2\pi f$ and
f is the signal frequency.

When terms in the equation 11 are being combined, becomes

$$V_{out}(t) = k_0 + \frac{1}{2} k_2 A^2 + \left(k_1 A + \frac{3}{4} k_3 A^3\right) \cos \omega t$$

$$+\left(\frac{1}{2}k_2A^2\right)\cos 2\omega t+\left(\frac{1}{4}k_3A^3\right)\cos 3\omega t \quad (12)$$

Equation (12) includes just second and third order harmonic distortion components but is applicable for higher order terms as well. Together with fundamental frequency ω, additional frequency components (2ω, 3ω..), whose amplitude depends on power series nonlinearity coefficients and input amplitude, are being generated. These additional frequency components are called harmonic distortion components which are illustrated in the Figure 5. These distortion components are usually located far away from the fundamental signal, thus not really effecting much on PA performance. However, they need to be filtered out to prevent them from interfering other systems. Unlike the even order nonlinearities, odd order nonlinearities also generate distortion into the fundamental carrier frequency ω [17]. [15]

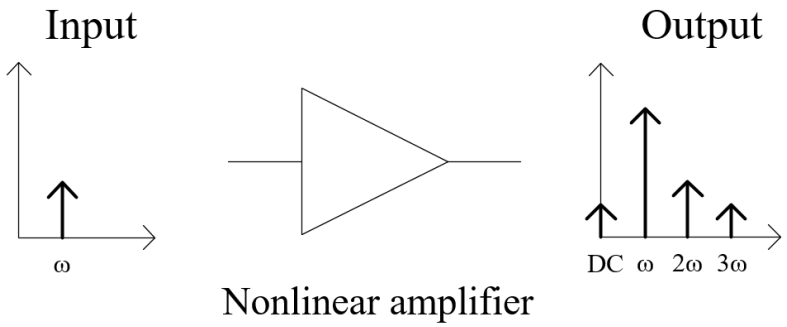

Figure 5 Harmonic distortion components.

4.3.2. IMD, Intermodulation distortion

When the amplifier becomes nonlinear and gets compressed, it will also produce mixing effect of two or more signals. In case there are multiple input signals fed to the nonlinear amplifier input, instead of one which was presented in the section 4.3.1, there are additional distortion components to be produced to the output spectrum. These intermodulation distortion components appear in addition to harmonics frequencies, and are dependent on the nonlinearity rate of the amplifier as well as the frequency and amplitude difference between these two input signals. This two-tone test is commonly used for determining the linearity performance of the power amplifier. [17]

If there are two signals having same amplitude fed to input at frequencies of f_1 and f_2, due to power amplifier nonlinearities there will be additional frequency components formed to the output according the following formula

$$f_{im} = mf_1 \pm nf_2, \quad (13)$$

where m and n are positive integers (including zero) and m+n determines the order of intermodulation distortion product. These additional distortion products are visualized with blue color in the Figure 6.

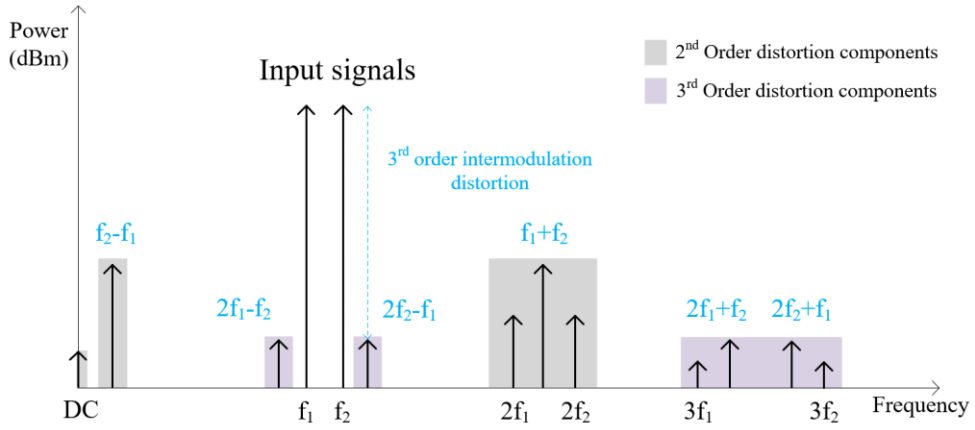

Figure 6 Intermodulation distortion products produced by nonlinear amplifier.

It is seen from Figure 6 that the intermodulation distortion products are, like harmonic distortion products, usually located far away from fundamental frequencies hence easily to be filtered out. Still, there are odd order intermodulation products which are formed just next to desired signals of which the products of most interest are the third order products ($2f_1$-f_2 and -f1-(-$2f_2$)). There might be components within the amplifier bandwidth which cannot be filtered out. Therefore, the relationship between IMD3 amplitude and fundamental amplitude (in dB) is important property for determining the nonlinearity of the power amplifier. Higher order contributions can become evident when operating in high compression due to their effect on third order amplitudes too. [17][18]

In case there are wide bandwidth modulated signals that consists of multiple frequency components fed to the input, also intermodulation products are having a wider bandwidth. It is then called spectral regrowth, and adjacent channel power ratio (ACPR), which is presented in Figure 7, is used as a measure instead of IMD3. Therefore, it is important to know mechanisms behind the ACPR properties and two-tone test over wide range of different tone spacings, covering whole signal bandwidth, is good for discovering amplifier capability. [16][19]

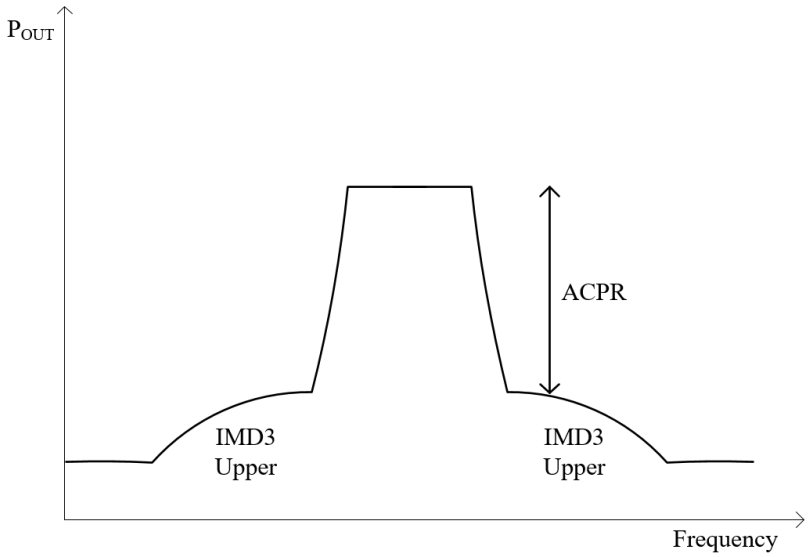

Figure 7 Adjacent channel power ratio.

4.3.3. Dynamic range

Dynamic range is a common measure for the linear capability of the amplifier. As can be observed from the (12), the more power is fed to input signals, more and more power is also spread to harmonic and third order intermodulation distortion products. Because of this, gain at the fundamental frequency decreases due to fact that total available output power is always finite. Ultimately this leads to the saturation of the amplifier. [16]

The linear region is located at the lower input power levels where the output is linearly proportional to the input. When the input power is increased enough, the real-life output response starts to differ from the corresponding linear one, and the amplifier compresses. The point where the difference to ideal response is 1 decibel is called 1-dB compression point, P_{-1dB}. The range between the noise floor and slight 1dB compression is commonly referred as the dynamic range of the amplifier. The point where theoretical linear extensions of fundamental and 3rd order distortion product intersect each other is called third order intercept point (OIP_3 if read from the output axis), which also describes the linearity by indicating how large signal amplifier can process before IMD occurs. Interception point is typically 10 dB above the 1 dB compression point which is well explained in [14]. [16]

The transistor ultimately enters to the saturation region P_{Sat} where the output power is not increasing anymore even though the input power is increased. Linearity properties can be improved if amplifier is driven in power back-off, but drawback is worsened efficiency. Figure 8 presents the behavior of the fundamental signal and third order intermodulation product as a function of the input power.

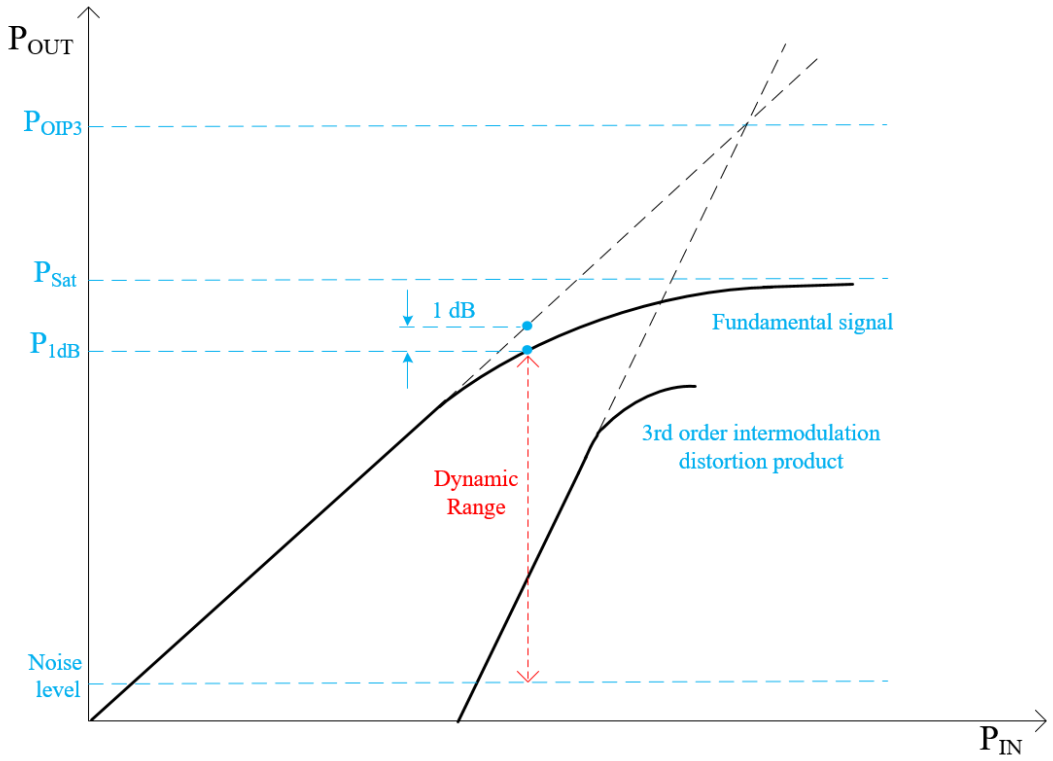

Figure 8 Dynamic range and interception point.

4.3.4. Amplitude and phase conversion

Another way to measure the existence of nonlinearities in the power amplifier is amplitude conversions that present the change in gain and phase properties of the fundamental signal as a function of input power. While the input power increases and amplifier gain starts to compress, signal peaks start to be clipped because the saturation region is being achieved. As can be observed from the (12), odd order nonlinearities start to modify the linear behavior of the fundamental signal amplitude too after a certain amplitude level is achieved. Even though the gain normally decreases (modelled by a negative k_3), it can occasionally exhibit a gain expansion where amplitude increases within certain input power levels, which is modelled with positive k_3 [20]. This amplitude-to-amplitude (AM-AM) conversion, which illustrates the amplitude dependent gain of the fundamental signal, is presented in Figure 9.

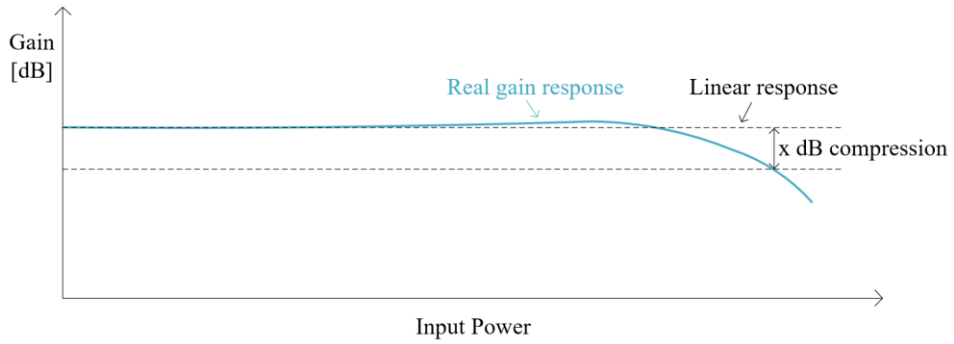

Figure 9 Amplitude conversion.

Amplitude-to-phase (AM-PM) conversion illustrates the phase distortion and defines how much the phase of the output signal changes as a function of input power. The better linearity properties amplifier has, the closer to compression point the phase gets distorted. Phase distortion can be harmful in modern modulation schemes that use phase information. Unfortunately, it is not always clear that how much distortion is allowable or what kind of response is feasible in terms of Digital Pre-Distortion (DPD) correction performance, and the origin for AMPM distortion is also a good deal of mystery. In general, they can be traced to signal level dependency of key transistor design elements, such as nonlinear resistances and reactance, and therefore there are good amount of differences in phase responses between different transistor vendors. Phase distortion is presented in Figure 10. [14]

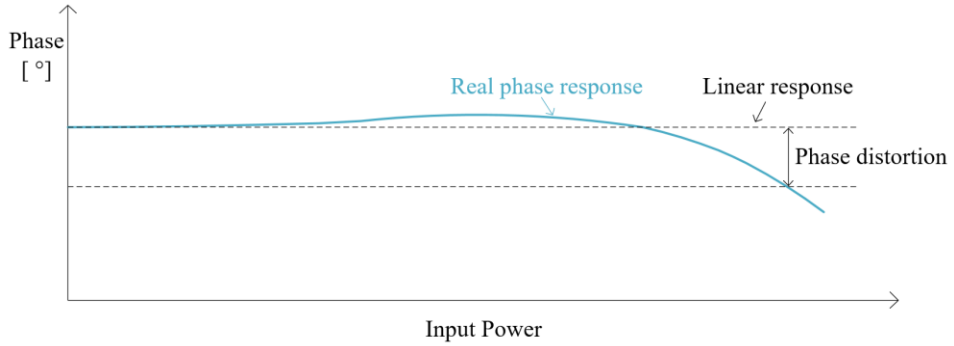

Figure 10 Phase conversion.

The drawback in use of conversion analysis as figure of merit for nonlinearity is that the measurement is generally performed using CW (zero bandwidth) signal at the fundamental frequency (which includes a strong linear term) thus altering AM-AM and AM-PM measurements highly sensitive to measurement errors. It also disables the effect of bandwidth and junction temperature dependent memory effects which will be introduced in the next section. Amplitude conversions, however, are also possible to measure with modulated signals nowadays, making them capable to also model memory effects in case the output samples can be synced to correspond the input symbols. [15]

4.3.5. Memory effects

Circuit elements such as coil, capacitor and all sort of active components store energy which is then detected as a memory effect. Therefore, the output response is not only based on the instantaneous input quantity but also previous stages affect. General nonlinearities generate new spectral components while memory effects shape these existing signal components. In power amplifier applications, the memory effect occurs if the input signal has wide bandwidth and variation in amplitude which is the case with modern communication signals and modulation methods. However, this may be misleading if the nonlinearity is modelled with polynomial expression (9) which shows only the effect of input signal amplitude and excludes the tone spacing.

There are two types of memory effects classified: electrothermal memory effects and electrical memory effects which are introduced in Figure 11. The difference between them is that electrothermal memory effects typically appear at low envelope frequencies (or modulation frequency) (KHz range) and electrical memory effects at higher, MHz range, frequencies. Yet another, especially GaN (Gallium Nitride) transistor technology related effect, is electron traps which are located between the active channel and the substrate. [15][20] [21]

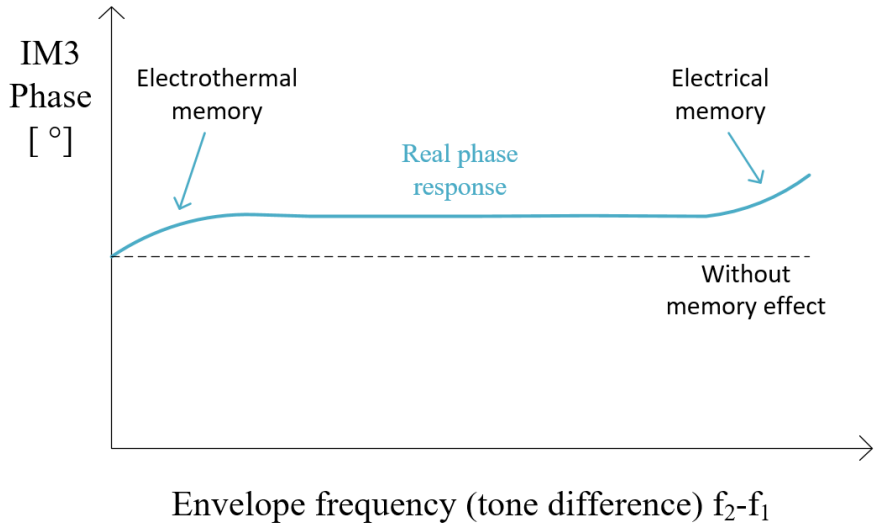

Figure 11 Phase response as a function of envelope frequency to illustrate the existence of memory effect.

Memory effects are seen as spectrum asymmetries, where lower and higher intermodulation distortion products are having different amplitude even though they are supposed to be the same according to equation (9). If the nonlinearity is modelled with applying two-tone signal to the 3rd order polynomial model, output amplitudes of IM3 sidebands can be written as

$$IM3 = \frac{3}{4} * k_3 * A^3 \tag{14}$$

from where it is noticed that the amplitude of IM3 product increases to the 3rd power of the input amplitude A according the polynomial model. If the polynomial model is extended to model 5th order nonlinearities too, it is noticed that as soon as the signal amplitude increases enough to cause this higher order nonlinearity, it affects the level of third order intermodulation product too and is called amplitude dependent memory.

However, the real-life response is a function of signal bandwidth, as said, and the existence of memory effect can be examined with real-life two-tone test where tone spacing refers to envelope frequency and equals to input signal bandwidth. The real phase response of IM3 product, which is seen in Figure 11, starts to deviate in dependence of envelope frequency leading also amplitude to change. It is important to remind that intermodulation distortion itself is not a memory effect, but these asymmetries, which are due to changes in envelope frequency, are regarded as one. The composition of amplitude and phase distortion ultimately leads to spectrum asymmetries where lower sideband is having lower amplitude in real life IMD measurements, which is well explained in [20]. [15]

Specifically, asymmetry is caused by electrical memory effects, which is related to bandwidth limitations of matching networks and biasing circuits, specifically from them becoming reactive at certain envelope frequencies. This leads bias current to change, which then causes a reactive effect if the biasing circuit is narrowband (high impedance). Node impedances (gate and drain) are seen as parallel connection between biasing circuit, matching network and transistor's internal impedances. Third order intermodulation products are affected by impedances at envelope frequency f2-f1 and harmonic frequencies 2f1 and 2f2, because these frequencies are mixed with fundamentals. Therefore, by controlling impedances and ensuring there are not resonances at these frequencies, IM3 products can be reduced. It is found that as the carrier separation degrades and approaches the cutoff frequency of the bias circuit, spectrum is becoming more asymmetrical. It is usually difficult to keep impedance levels constant, especially in envelope frequencies, which can vary from DC to several megahertz and even more in the future. [16][19][20]

Thermal compensation circuits are used for keeping the DC drain current level constant and thus ensuring the transistor to operate in the wanted operating region. Electrothermal memory effect is caused by electro-thermal coupling in the transistor and is detected as gain variations when the transistor gets warm. Thermal impedance (expressed as °/W) describes the rise (or fall) in the transistor die temperature caused by dissipated power. If the thermal impedance is high, increased dissipation power is observed as a higher growth in the transistor die level temperature. This leads to existence of temperature power feedback (TPF) because the amplifier gain is dependent on the die temperature. Thermal impedance is not purely resistive thus

producing a distributed lowpass filter that passes through the DC component and envelope frequency component of the dissipated power. [19][21]

Semiconductor trapping effects can be observed by monitoring the transistor channel current when the input voltage is switched from the cutoff region to linear conduction region. There might be huge difference in time constants with regard to settling time, which are due to trapped charge carriers. [14]

4.4. Linearization

Linearization is used when better linearizability performance is needed to fulfill strict and standardized specifications. Good efficiency is achieved with expense of linearity and there occurs distortion, seen as high adjacent channel power levels, when the transistor is operating in nonlinear region. To improve this trade-off, amplifier is designed for good efficiency with lower linearity properties, and then enhancing the linearity somehow to achieve both: good efficiency and linearity. This is implemented with help of different kind of linearization methods of witch digital adaptive pre-distortion (DAPD) method being the most common nowadays in base station applications. The 1dB compression point is generally considered as a design point where sufficient linearity is still maintained without linearization methods, but with help of linearization method this can be extended to 3dB compression point. [22]

Digital adaptive pre-distortion method is polynomial method, where the nonlinearity is modeled from the amplified output response via the feedback branch, and then counter-distorting the input baseband signal accordingly by adjusting power series coefficients (k_n in (9)) and phase quantities. In the other words, the baseband input signal is distorted in a way where distortion products are having equal amplitude but opposite phase compared to previously sampled output quantity. When it experiences the nonlinear amplification, the resulted amplified output signal is then as linear as possible where nonlinear products (IM3, IM5 etc.) are cancelled the most effectively. Digital adaptive predistortion method is presented in Figure 12. [19]

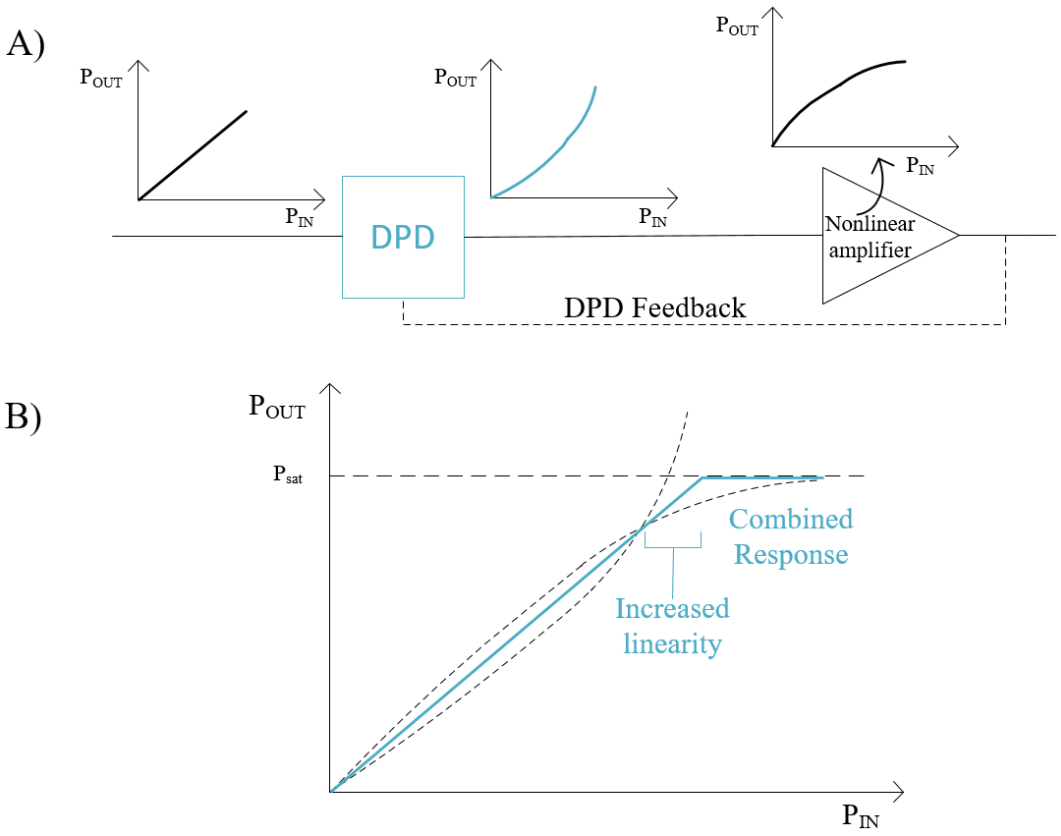

Figure 12 A) Digital Adaptive Pre-Distortion (DAPD) method and B) Produced output.

However, the challenge is that previously introduced memory effects cause variation in intermodulation tones by varying their amplitude and phase values. It thus makes predistortion modeling more difficult as there are additional dynamic PA effects that cannot be accounted to PA polynomial nonlinearity model. In consequence memory effects limit the linearization performance, but it is also challenging to model counter-distorted input signals accurately to match the distorted output response. To model memory effects, history information of applied signal is needed and memory polynomial modelling is required. Another issue is the fact that, in addition to nonlinear amplification, the distortion is occurred at the PA input and output too and in future mMIMO systems there may be crosstalk seen between the different signal paths. These cannot be compensated with conventional DPDs and crossover DPD (CO-DPD) modelling is needed [23]. With use of effective predistortion one can achieve good position in the markets where good efficiency is often steering the investments. [15]

In order to enable the DAPD functionality, a sample is needed to be taken from the output response for which directional coupler is usually used. Feedback signal is a lower power copy of the output response which is then fed to digital unit, but it also should be as pure copy of the output as possible. Therefore, in terms of this master's thesis, the removal of circulator most likely causes distortion to the output response (and therefore to the feedback too) due to reflective signal, but one of the key aspects is that does it affect too much.

4.5. Operating classes

Power amplifiers are divided into different operating classes according to operating point and conduction angle they are having. The operating point determination is carried out by biasing the transistor to the wanted off state condition, ie. the state when there is not RF signal applied to it. Biasing means that the gate voltage and drain current is set so that wanted operating point is achieved and therefore the operating principles of the transistor can be adjusted.

In terms of power transistor principles, especially the time when the transistor is not conducting is controlled by setting the operating point accordingly. This can be explained with conducting angle which determines the part of the signal period when the transistor is active and consumes power. The conducting angle and operating point together determines the operating Class for the transistor. The most common operating classes used in base station power amplifiers are Class A, B, C and AB and they are introduced in this chapter.

Class A amplifier, which is introduced in Figure 13, has the widest conduction angle (360°) and its operating point is located at the amplifier linear region. This means that the current flows even on the DC state when there is not any signal to be amplified leading. Therefore, class A amplifier has the worst efficiency capability within operating classes, maximum 50%.

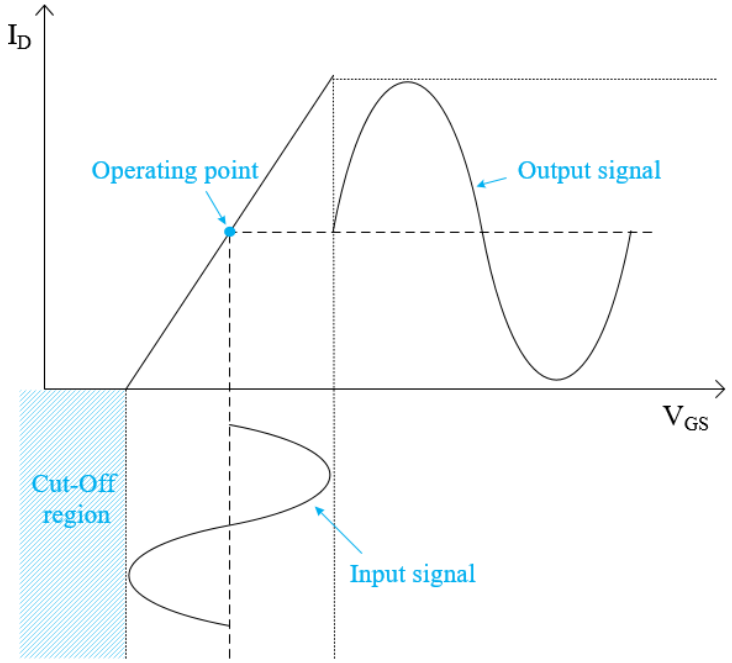

Figure 13 Class A amplifier.

The operating point of class B amplifier is set so that amplifier is not located at active region on DC state and consumes power only when the input signal power is above the set operating point. As seen in Figure 14, the conducting angle of Class B amplifier is 180° which means that it conducts only the positive halves of input signal leading to better efficiency at the cost of worse linearity. Theoretical maximum efficiency of Class B amplifier is 78.5%.

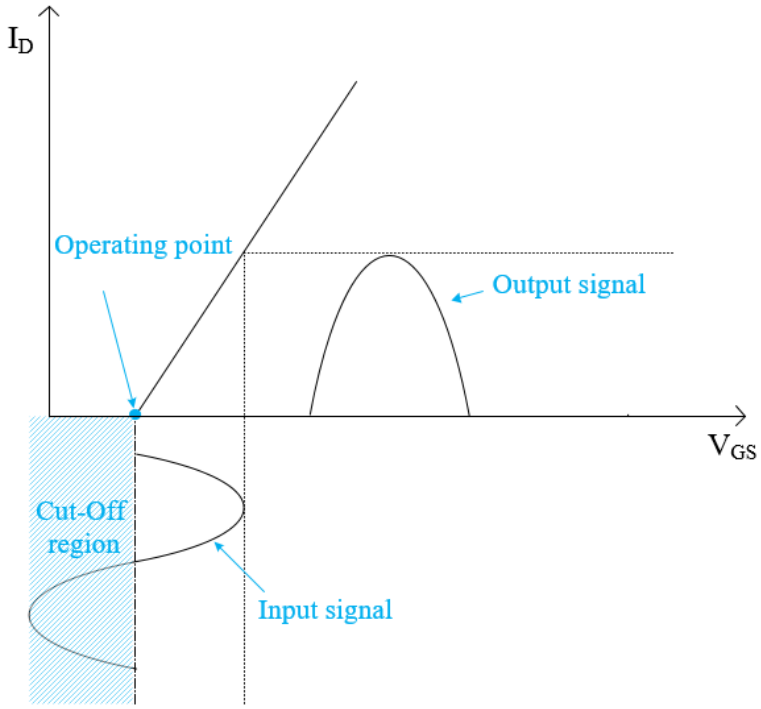

Figure 14 Class B amplifier.

Class AB amplifier is compromised between Class A and Class B amplifier. Operating point is set so that transistor remains at active region on DC state, but consumes less current compared to Class A amplifier. The goal is to combine the linearity capability of Class A amplifier with better efficiency capability of Class B amplifier. The conducting angle is between 180° and 360° while efficiency is between 50% and 78.5%. Class AB amplifier is presented in Figure 15.

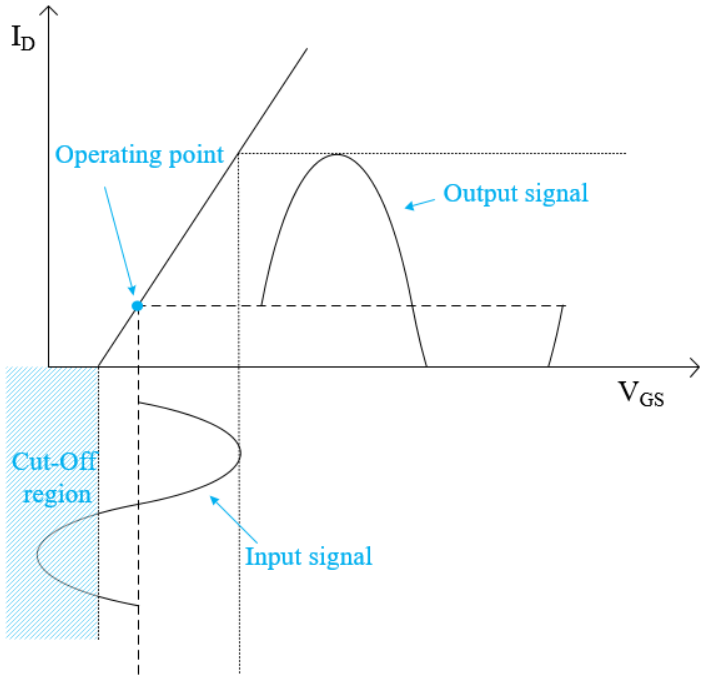

Figure 15 Class AB amplifier.

Operating point of Class C amplifier is set lower compared to Class B amplifier, and amplifier is not consuming current on DC state. Conducting angle is also clearly below 180° of Class B amplifier as seen in Figure 16. Of the operation classes presented here, Class C amplifier owns clearly the best efficiency capability, while linearity is the worst. Class C amplifier is often used as peaking amplifier in Doherty structure, which is introduced later.

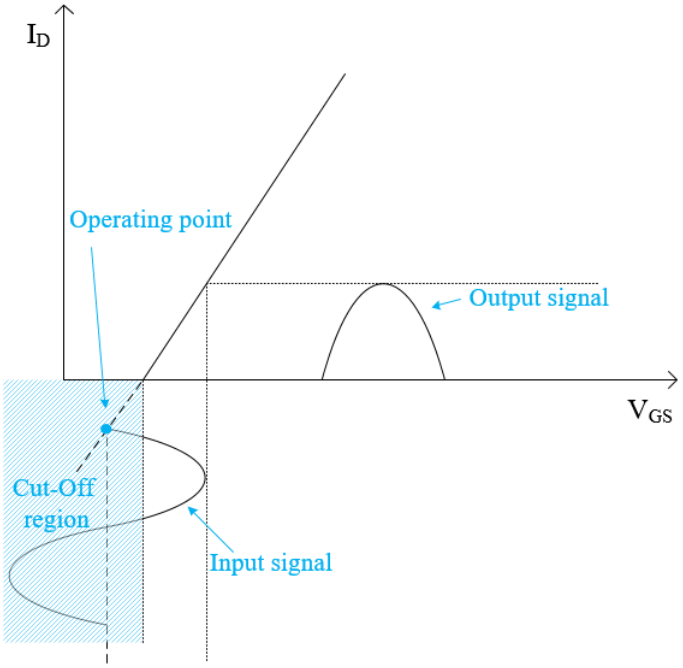

Figure 16 Class C amplifier.

4.6. Impedance matching

Maximum power transfer from a source to a load is achieved by matching load and source impedances together. In case they are not properly matched, portion of delivered power is reflected at the interface between the sections with different impedances, and therefore some power is lost. In practice, reflected power is defined by a power return loss which determines the amount of reflected power in decibels. Power return loss is determined with -20log(Γ), where Γ, reflection coefficient, is defined as

$$\Gamma = \frac{Z_L - Z_S^*}{Z_L + Z_S^*}, \tag{15}$$

where

Z_L is the load impedance and
Z_S is the source impedance.

Generally, the purpose of the matching is to match source and load impedances to the reference impedance which is usually 50Ω but in the PA world, the output is usually matched to impedance point that produces the maximum peak power capability.

Matching networks are implemented by using microstrip transmission lines and reactive components thus adapting impedances to the loads that are not purely resistive due to fact that there are internal capacitance and inductance in the RF power transistors which are needed to be compensated. In theory, maximum power transfer is achieved by using complex conjugate matching, where matching network is designed so that known load impedance is matched to 50Ω using complex conjugate point of the source impedance as a starting point in the smith chart. But in practice, the load impedance is often matched so that the wanted power level is achieved with the available voltage swing. Otherwise, because of the higher load impedance caused by the conjugate matching, power amplifier would saturate in lower power levels already, especially in lower V_{DS} voltage applications. It is preferable to use high Q, quality factor, reactive elements in matching circuits, because they provide wider frequency bandwidths. [24]

4.7. Transistor technologies

In the very beginning of the radio frequency power amplifier (RFPA) design there were two types of transistor technologies used, one based on silicon (Si) and one based on Gallium Arsenide (GaAs). As years went by, it seemed to be obvious that high power capable GaAs technology will hijack the microwave world above 2 GHz, despite its issues in reliability as well as material availability and the higher cost compared to Si. [14]

However, as the low-cost requirements in the wireless communications sector raised head in the late 1990s, high power cellular base stations were target when new Si technology was developed. Development was driven by Motorola and they developed Laterally Diffused Metal Oxide Silicon (LDMOS) technology, which has become the default choice for PA applications even up to 3 GHz nowadays. [14]

Alongside with the LDMOS technology, Gallium Nitride (GaN) technology has been developed during 21st century due to its high voltage operation and higher frequency capabilities. However, there are also high voltage LDMOS transistors developed today to fulfill the demand for higher power levels and thus provide higher power densities (W/mm) [25]. [14]

Transistor technologies evolve because some key properties are always tried to achieve: power, high gain, good efficiency and linearity, low cost and good reliability. One technology tends to dominate markets until a new technology offers a more compelling solution. In the near future, GaN transistors will more likely to replace LDMOS transistors as the wireless communication sector is evolving from LTE (Long Term Evolution) to 5G mmW frequencies. [13]

The most common circuit configuration for RF power amplifiers is the common source (CS) configuration, where the input signal gets amplified from gate to drain.

4.7.1. LDMOS transistor

LDMOS transistor structure consists of four terminals which are identified as source, drain, gate, and substrate. Due to n-type MOSFET construction, the drain is connected to the high DC voltage while the source is grounded. Thus, the gate induces a field-enhanced depletion region between the source and drain creating a channel between them. Current flows laterally near the surface which allows easy current optimization and makes it capable for high frequency operation where also high efficiency is wanted. [13]

Cross-section of LDMOS die is shown in figure 17. There is lightly doped n-type drift region "n-drift region" (NHV) between the drain and gate connector. The length for the n-drift region is determined by drain-source voltage V_{DS} and larger the drain voltage is, longer is the n-drift region. When a positive voltage above the threshold level, with respect to the source, is applied to the gate and V_{DS} voltage is large enough, transistor works in active region. Then the channel is opened between the n-type drain and n-type source, and current flows from drain to source via the channel. Threshold voltage level and turn on characteristics of the device are determined by PHV region properties. [13]

Appropriate length and doping concentration for n-drift region is determined together with V_{DS} determination. Traditionally length varies from 0.5 µm with lower drain-voltage to 6µm with higher drain-voltage. Major high-power RF applications are designed with V_{DS} supply voltages of 32 V or 50 V. The purpose of the n-drift region is to ensure that the drain region potential below the gate is low enough and preserve the integrity of the gate oxide. The length of lightly doped n-drift region determines the breakdown voltage level between the drain and source connectors which is usually enabled to reach twice the supply voltage level. [13]

A low doped n-drift region reduces the Hot Carrier Injection (HCI) which is found to be one of the problems concerning LDMOS technology. HCI means that there are high energetic carrier electrons that get stuck to gate oxide (usually SiO2) due to high electric fields. This causes threshold drift over the years. [13]

RF LDMOS transistors are unique in terms of source electrode structure. The source of the transistor consists of two same potential terminals as the bottom metal layer is also connected to source terminal via the low resistance p+ doped sinker and p+ doped substrate. This allows RF LDMOS transistor to be soldered directly to ground minimizing the wiring parasitics, leading to smaller common source impedance and enabling better thermal conduction because the transistor can be integrated to the mechanics. Because the source electrode is located at the bottom layer side of the transistor, drain and gate electrodes are located at the top. This structure enables to design specific grounded conductor (so called field plate) close to n-drift region that provides an additional freedom for optimization of the n-drift region properties. The grounded field plate also reduces subsurface electric field and acts as a shield between the drain and gate electrodes leading to smaller gate to drain feedback capacitance and parasitic drain resistance. This, together with smaller source wiring inductance and drain to source capacitance, leads to higher power gain, bandwidth and power density and enhances stability. [13][26]

One of the benefits concerning the LDMOS transistor is that its drain current temperature coefficient changes from positive to negative as current increases towards more useful operating currents thus preventing transistor from breakdown. In addition to that temperature stability is found to be relatively good nowadays. Due to fact that

there is no gate current at all, the gate DC impedance is high. This allows relatively simple biasing circuits but on the other hand impedance matching is quite difficult to implement. [13][26]

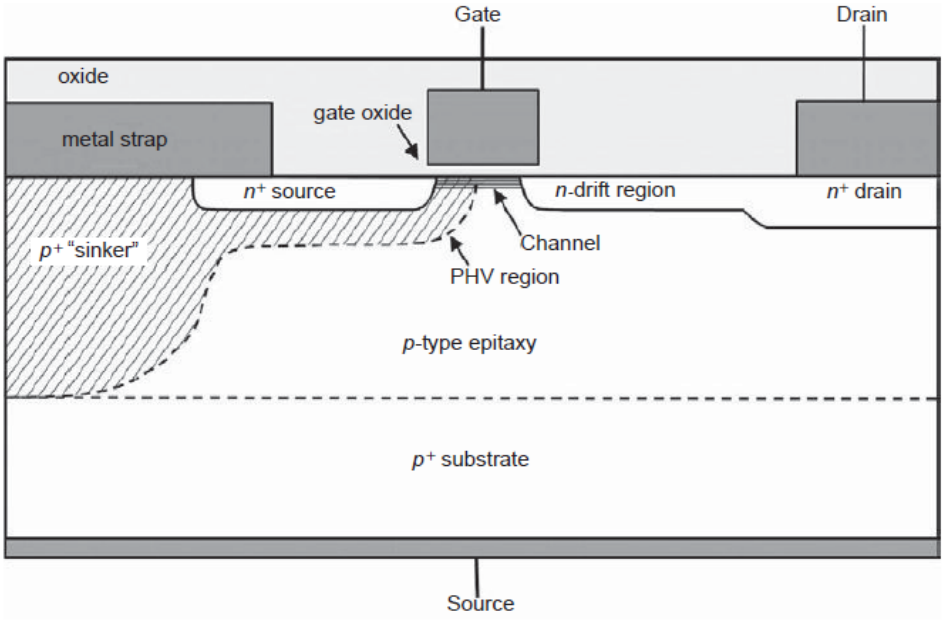

Figure 17 LDMOS transistor cross section.

4.7.2. GaN transistor

During the years in 20th century, it has been under a great interest to find RF power transistors solutions with wide bandgap semiconductors. Gallium Nitride (GaN) has been the most promising candidate for high voltage applications and higher millimeter wave frequencies with increased bandwidths. The GaN based materials have energy bandgap about two to three times larger than tin conventional semiconductors such as Si and GaAs. The power density is also about twice compared to traditional Si technologies, 6-12 W/mm compared to 1-5 W/mm, and provides better PAE (Power Added Efficiency) which allows smaller devices. The natural capability for higher operating voltages makes GaN transistors fascinating as they offer better efficiency for power amplifier, thus leading to simplified cooling too. However, higher power densities are often achieved under high gain compression of 5-9 dB, which indicates to undesired nonlinearities. This is found to be due to trapping effects, and is under development before they are deployable in future base station applications. [14][13]

GaN transistor technology is very much like LDMOS technology in power amplifier deployment perspective, but the most obvious difference is that the negative gate control voltage is essential.

5. POWER AMPLIFIER TOPOLOGIES

Doherty topology, which has originally been introduced in the mid-1930s by William H. Doherty, is widely used in today's base station power amplifiers. It is designed for enhancing the PA efficiency at back-offed power levels where efficiency is usually just tens of percent with conventional type class A amplifiers. It is vital to enhance the efficiency at back offed power levels, because todays modern modulation schemes together with wideband signals have high peak to average ratio (PAR) which are needed to be driven below compression. [14]

5.1. Classical Doherty topology

Even though the power amplifiers are most likely to be implemented into the small sized modules with future mmW frequencies, they are often Doherty structures inside and it is vital to know what is located "under the hood". The Doherty amplifier is implemented by combining the class B or class AB biased amplifier for operating at lower power levels and class C biased amplifier for supporting the main amplifier at higher power levels. They are being named as main (carrier) and peaking branches accordingly. The classical two-way Doherty topology is illustrated in figure 18 which incorporates amplifiers that are separated by quarter wave transformer (key part for so called load modulation technique), and another transformer at the peaking side input to compensate the 90 ° phase shift introduced by that output transformer. [18]

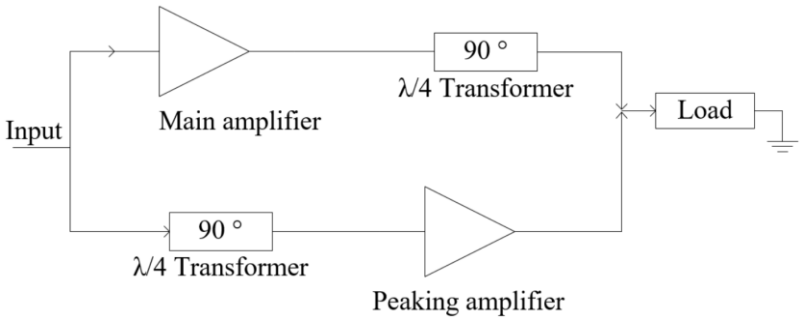

Figure 18 Doherty topology block diagram.

The Doherty amplifier operation is based on so called load modulation method, named also as an active load-pull technique, in which load impedance seen by the main amplifier changes in correlation to operating power level. Doherty amplifier circuit diagram is illustrated in figure 19 from where the node impedances can be solved.

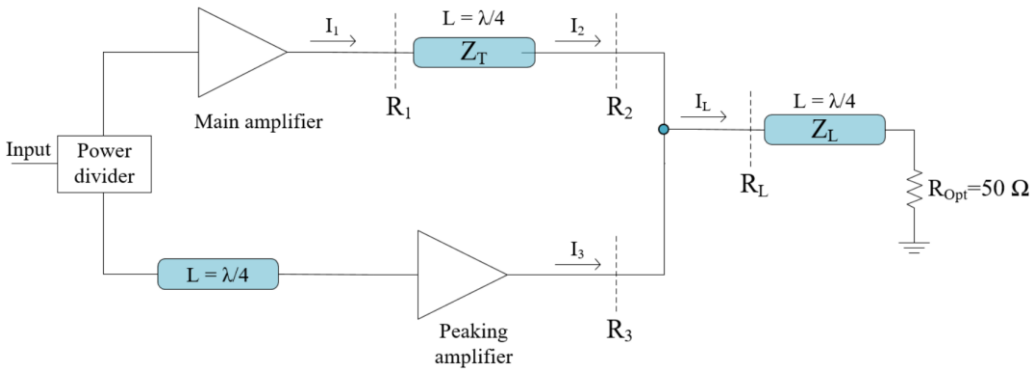

Figure 19 Doherty topology with node impedances and currents.

The quarter wave (λ/4) transformer, named as an impedance inverter, at the output of the main branch plays a big role here by enabling the load modulation. Its ability to invert the impedance is characterized with the following equation

$$Z_T = \sqrt{R_1 * R_2}, \tag{16}$$

where

R_1 is the output impedance seen by the main amplifier,
R_2 is the output impedance seen by the main branch and
Z_T is the transmission line impedance.

Transmission line impedance Zt is kept constant in Doherty amplifier topology which leads main amplifier output impedance to be

$$R_1 = \frac{Z_T^2}{R_2} \tag{17}$$

The actual main branch load impedance R_2 can be expressed with two equations by noting node voltages from Figure 19.

$$V_{R2} = R_2 * I_2 \tag{18}$$

$$V_L = R_L(I_2 + I_3) \tag{19}$$

Equations 18 and 19 equals together, which leads to

$$R_2 = R_L \frac{(I_2 + I_3)}{I_2} \tag{20}$$

Now the output impedance of the main amplifier, R_1, can be calculated by substituting R_2 in (17)

$$R_1 = \frac{Z_T^2}{R_2} = \frac{Z_T^2}{R_L} * \frac{I_2}{(I_2 + I_3)} \tag{21}$$

Generally, impedances are kept constant in the Doherty topology by dimensioning quarter wave impedance Z_T to R_{OPT} and load impedance R_L to $R_{OPT}/2$. Also by substituting I_2 with I_1 due to lossless property of the transformer, (21) can again be simplified to

$$R_1 = 2R_{OPT} * \frac{I_1}{I_1 + I_3}, \tag{22}$$

Where

R_1 is the output impedance seen by the main amplifier,
R_{OPT} is generally considered 50 Ohm,
I_1 is the main branch current and
I_3 is the peaking branch current.

From there it is seen that the load impedance seen by the main amplifier changes as a function of peaking amplifier current and therefore the principle of the Doherty concept can be explained by dividing it into two cases, where the 6 dB back off point is used as a boundary. The behavior of the main and peak amplifier drain voltage and current is illustrated in following figure as a function of the input excitation signal.

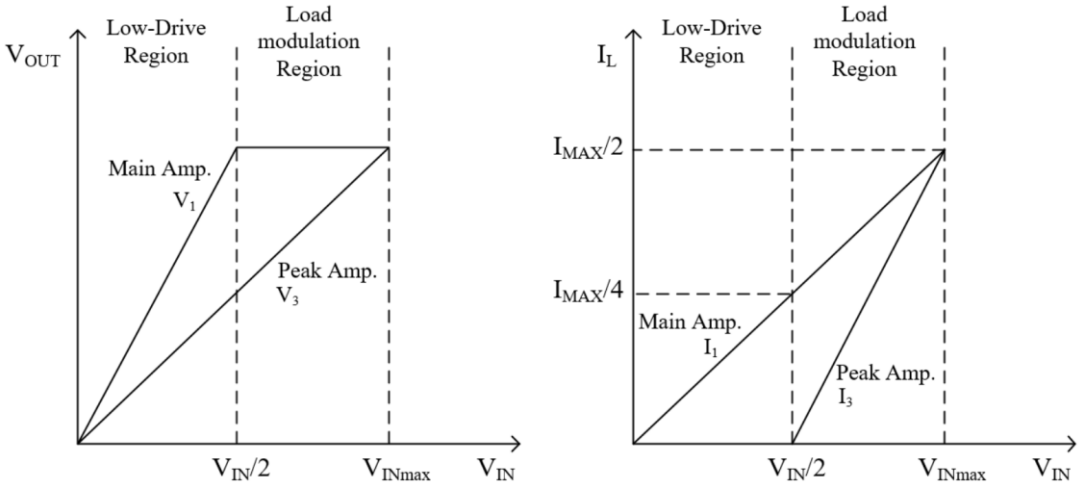

Figure 20 Basic principle of Doherty topology.

First, at the lower input power levels, the peaking amplifier is not generating RF power and I_3 is zero. Therefore, a load impedance seen by the peaking amplifier is infinity according to ohms law. At the same time, the main amplifier operates into a load impedance $R_1 = 2R_{OPT}$ as seen in equation 22. Determination for low power zone depends on peaking amplifier biasing conditions but is usually defined to Pmax/4 (6dB threshold point). Main amplifier current maximum is $I_{max}/4$ at low power levels, where the input voltage maximum is $V_{IN,max}/2$ and the output voltage has reached its maximum. Main amplifier starts to saturate in the 6dB threshold point and the linearity performance is just maintained by the main amplifier capability until that.

Then with higher power levels, above the peaking amplifier threshold level when the input voltage increases from $V_{INmax}/2$ towards the V_{INmax}, the functionality of the impedance inverter is seen. According to (20), as the peaking branch current I_3 increases also the main branch output impedance R_2 increases. However, thanks to impedance inverter functionality, the main amplifier output impedance R_1 then decreases from $2R_{OPT}$ towards the R_{OPT} as seen in (22). While the main amplifier output impedance decreases, but main amplifier output voltage has already achieved its maximum, main current I_2 also increases together with the peaking current I_3 as the power is saturated in the main branch. If the maximum of the load current I_L is denoted as I_{MAX}, the maximum branch currents I_2 and I_3 are $I_{MAX}/2$ each. Ultimately, when both branch currents have achieved their maximum values at the maximum power level, all impedances (R_1, R_2, R_3) are found to have same value, R_{OPT}.

Outputs are then combined and fed to the R_{OPT} 50 Ω load through an impedance inverting network Z_L, which is also a quarter wave (λ/4) transmission line. This impedance inverter is required to match the Doherty amplifier to standard 50 Ω load because the node impedance R_L (when looking towards the Doherty transistors) is 25 Ω no matter if the peaking side is conducting or not. [14] [27]

The combined performance of the main and peaking side, thus also the deepest principle of the Doherty technology where the good efficiency performance is maintained in backed off levels too, is illustrated below in the output power and efficiency figure. From there it is seen that the efficiency capability is contributed by the main amplifier until the output power back off point (E.g. -6dB), and maintains the performance until the peaking amplifier starts to support the performance.

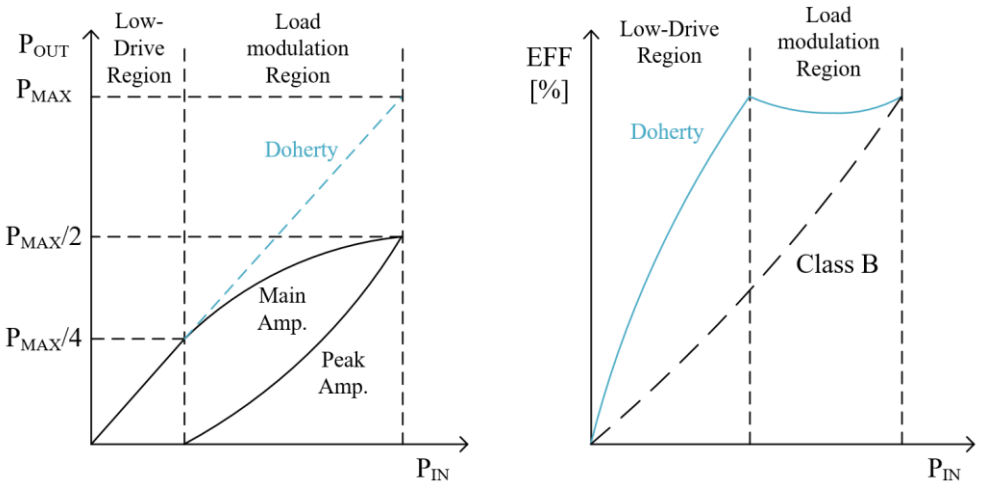

Figure 21 Two-way symmetrical Doherty structure power and efficiency performance.

5.1.1. Developed Doherty structures

The structure which was introduced in chapter 5.1 is called symmetrical two-way Doherty. There both, main and peak side, transistors are having same power characteristics and therefore the efficiency optimization can be implemented with different biasing conditions. However, again higher back off efficiencies are needed when modern communication signals with even higher peak to average ratios (PAR) are used, and therefore new topologies have been developed.

5.1.2. Symmetrical three-way Doherty

There are still couple other options for fulfilling the requirements of higher PAR signals. One is to use transistors with higher power characteristics in symmetrical two-way Doherty structure and thus fulfil the peak power requirements. The drawback there is that the main transistor efficiency performance is then lost due to less efficient power range usage. Another option would be to use more transistors in parallel (three-way Doherty) where two peaking amplifiers are used instead of one [28]. The drawback there is higher cost, bigger overall size and more difficult matching. The comparison between two-way and three-way Doherty is illustrated in the Figure 22 from where it is noticed that higher efficiency can be maintained over the larger back-off range with three-way structure.

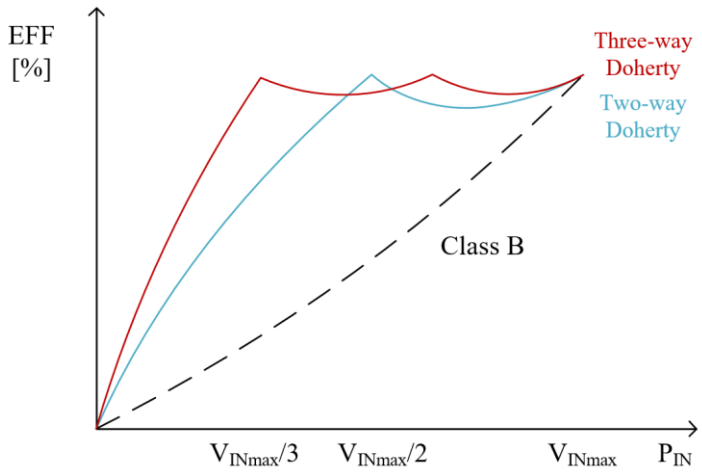

Figure 22 Comparison between two-way and three-way structure.

5.1.3. Asymmetrical Doherty structure

Due to three-way Doherty drawbacks, asymmetrical Doherty structure has been developed for extending the efficiency over a wider range of output powers [28]. The asymmetrical structure can be implemented two ways: either by using asymmetrical power divider at the input of the Doherty structure for coupling higher amount of power to peaking side or then by using different sized transistors in main and peak branch. The lower power characterized transistor is used in main side amplifier and higher power capable transistor in peaking side. Usually implementation is compromise where both, asymmetrical power divider together with different power characterized transistors, are used. The asymmetrical Doherty efficiency plots are illustrated in Figure 23, where the extended power back off capability can be seen.

Equations for the impedance levels, which are introduced in the chapter 5.1, are not valid anymore as the current division ratios have changed due to different transistor sizing. However, equations which are applicable to asymmetrical structure are not presented here.

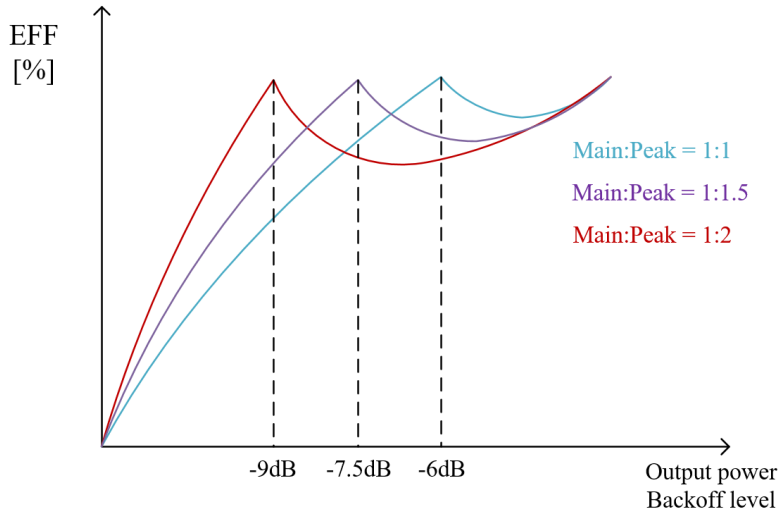

Figure 23 Asymmetrical Doherty structure and its effect on efficiency performance.

5.2. Balanced structure

Balanced structure is composed of two amplifier units that have equal properties and performance. They are arranged between 3 dB 90° hybrid couplers which act as the input splitter and output combiner where both are causing 90° phase difference between the coupled and through port. The input signal is first split into two equal amplitude components (-3 dB but another 0° phase shifted and another 90°) which are then amplified and finally recombined by another oppositely connected quadrature coupler leading output to be amplified sum of the input. Balanced structure provides improved input and output matching, gain flatness for a wide frequency range and adds ruggedness as the PA is still able to function even if one of the amplifiers fails. It is also beneficial in terms of previous stage conditions because the possible reflections, which are occurred due to poor amplifier input matching, flow into the isolated port and dissipate on the termination resistor.[27]

The drawback is commonly stated to be the higher price which is due to addition of twice number of components compared to single ended structure. Moreover, the overall size is thus larger and efficiency is worse. On the other hand, to achieve the same power capability with single ended structure, transistor having twice the power capability of each used in balanced structure is needed. The other way around, if the same transistor which is employed in single ended structure is used in balanced configuration, 3 dB higher output power and OIP3 (shown in Figure 8) is achieved. Balanced power amplifier configuration is presented in Figure 24. [22]

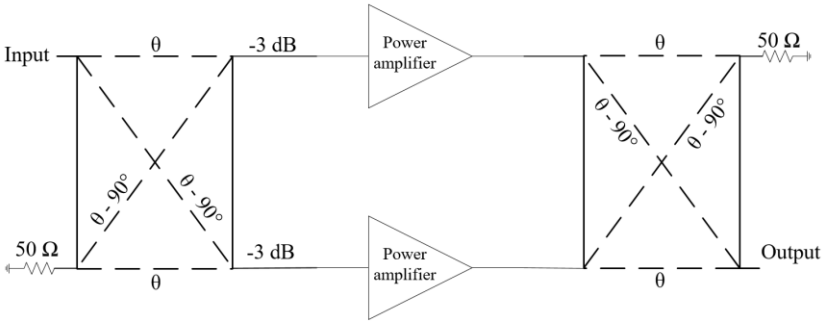

Figure 24 Balanced amplifier configuration.

6. IMPLEMENTATION

6.1. Proposed power amplifier design for 5G mMIMO TDD base station

One possibility for overall PA section size, cost and efficiency enhancement could be to remove the large sized lossy component, circulator, from the RF path and replace it with RF switch for the TX/RX separation in the TDD base station.

However, the removal of the circulator will lead to fact that practically frequency independent stable load provided by the circulator will be then changed to the load which is highly frequency and antenna array configuration dependent, as explained in chapter 3 "5G Massive MIMO Base station". It is difficult to ensure proper load properties in a PA perspective which may lead to overall performance degradation with certain mMIMO functionalities where the variation especially in peak power and efficiency capability over the bandwidth might be evident. This is because the optimum PA performance is generally achieved against the known load via the specifically designed matching network. In the other words, the amount of nonlinearity is affected, as the point where amplifier becomes nonlinear changes according to load impedance. With the high load impedance amplifier compresses sooner than with the low load impedance.

In addition to active load to which PA is then exposed to, there will not be any elements available in RF chain which would absorb the reflected wave travelling towards the PA output and power amplifier becomes susceptible to reflections. Moreover, not only load mismatch related reflections exist, but also coupled signals from surrounding elements are to be summed. This is illustrated in the Figure 25 where V_{PAn} is the amplified incident output signal of the TX branch "n" and V_{REn} is the reflected wave correspondingly. The reflected wave is composed of load mismatch related reflection and coupled response from nearby surrounding elements. Reflected wave travelling towards the PA output of the n^{th} TX branch can be expressed as follows: [29]

$$V_{REn} = S_{nn}V_{PAn} + \sum_{k=1}^{K} S_{nk}V_{PAk}\,, \tag{23}$$

where

$n \geq 1 \; and \; k \neq n$,
S_{nn} is antenna input return loss S-parameter,
S_{nk} is the S-parameter for coupling from neighboring antenna elements and
V_{PAk} is the incident wave of each neighboring element.

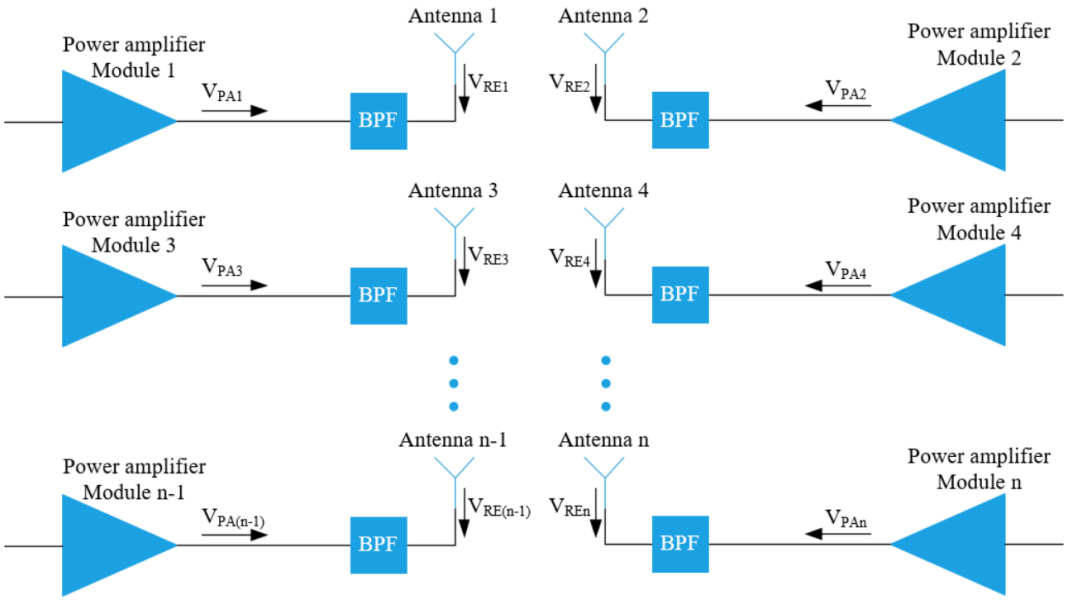

Figure 25 Massive MIMO block diagram from power amplifier section onwards.

Hence the drawback in circulator removal is that all possible reflections will then be travelling all way back to the transistor output and might even broke the amplifier block if the reverse power gets too high. However, in case there is totally broken load and unity reflection, there should be some specification defined for the transistor vendor that how long the transistor should endure the reverse power. This is usually base station software level specification too, and as soon the ultimately bad load is noticed, the base station should stop transmitting via that TX branch.

In addition to reverse power endurance, probably the most significant arising unit level issue to be concerned about is the effect of reflections and changing load properties on the Digital Adaptive Pre-Distortion (DAPD) performance. Feedback response for the pre-distorter is supposed to be exact copy of the amplified PA output signal thus imaging the nonlinearities produced by the nonlinear amplifier which are then to be linearized. The DPD performance, however, will be most likely degraded due to multiple reflections, which are occurring simultaneously between the PA output and antenna input. Therefore, removal of the circulator may lead to situation where the feedback is not exactly modelling the PA nonlinearities only and the feedback response quality becomes proportional to the Voltage Standing Wave Ratio (VSWR) at the PA output. [30]

Not only cost effectiveness is advocating the circulator elimination, but again the natural feature of mmW frequencies also give its own requirements. Migration to higher frequencies causes higher cable and PCB transmission line losses and therefore it is essential to place RF parts closer to antenna elements in high integration leveled mMIMO structures. By doing so, the signal attenuation and distortion between the amplifier stage and transmitting antenna is minimized.

After all, if the circulator removal is realizable with reasonably good performance over the total bandwidth, smaller PA size together with cheaper bill of materials (BOM) price for the PA section will be achieved. These particular challenges will be investigated in this thesis with help of simulations and physical implementation.

6.2. Requirements

The original power amplifier design, which is used as a reference design in this thesis, is part of coming Nokia TDD mMIMO product that includes 16 TX/RX paths which are designed to work in 3.4-3.6 GHz frequency band. The power amplifier implementation was decided to be performed with Ampleon integrated Doherty LDMOS transistor lineup which is then analyzed and evaluated with and without the circulator against the real load properties provided by the filter and antenna array used in Nokia base station products. Balanced structure was used for both reasons: to meet the specification in the peak power requirement perspective as the single ended demo structure did not have enough, and to enable better protection against the changing load in the PA perspective. The block diagram of the power amplifier implementation used in this thesis is seen in the Figure 26.

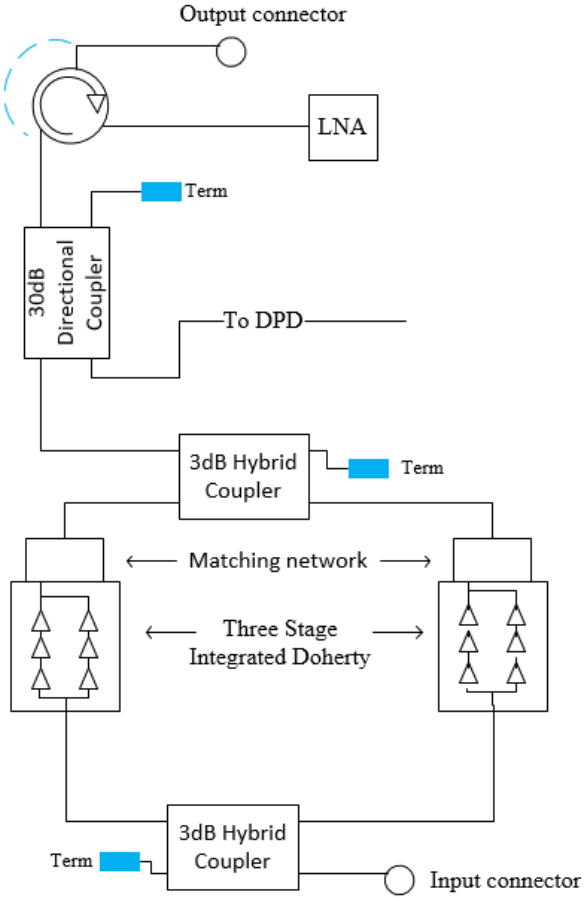

Figure 26 Power amplifier section used in this thesis. Dashed line denotes the circulator bypass.

Specifications for power amplifier section are as follows: power amplifier nominal output power 39.5 dBm including isolator loss of 0.5 dB, minimum total lineup gain 42.5 dB, total efficiency larger than 40%, 3 dB compression point at the output power of 48.5 dBm at which phase compression maximum 25°. However, as only the final stage is analyzed in this thesis, gain requirement is not relevant.

Traditionally PAs are considered to need to be provided with better than -20 dB input return loss load conditions. Otherwise the PA performance will degrade, and for that purpose circulator is placed at the output: to provide stable and good load property.

Based on experience of my colleagues, in addition to natural variation in antenna load condition, the antenna element input return loss might worsen approximately 2 dB more as a function of beam steering action. This, together with antenna element coupling, will most likely cause higher VSWR to PA output in case the circulator is removed, as explained in (23). There are also specifications for gain flatness, which is 1.5 dB within the frequency band, and digital predistortion feedback response ripple which is generally considered to be 1dB at max. Therefore, due to higher VSWR, these responses might get distorted too. These requirements are evaluated with help of simulations and hardware measurements, and are presented in next sections

6.3. Implementation workflow

Deep and close co-operation with Nokia antenna design team, filter design team and transistor vendor was needed when investigating the behavior of the power amplifier under a varying load condition and effect of the circulator removal on the PA RF performance. The work started with discussion sessions together with antenna design team members to achieve better understanding and to get proper simulation model for our needs concerning the coupling effect simulations. This was crucial and essential for completing the rest of the work, as the load points that were observed in simulations were later used in the hardware measurements. Implementation workflow is presented in following block diagram.

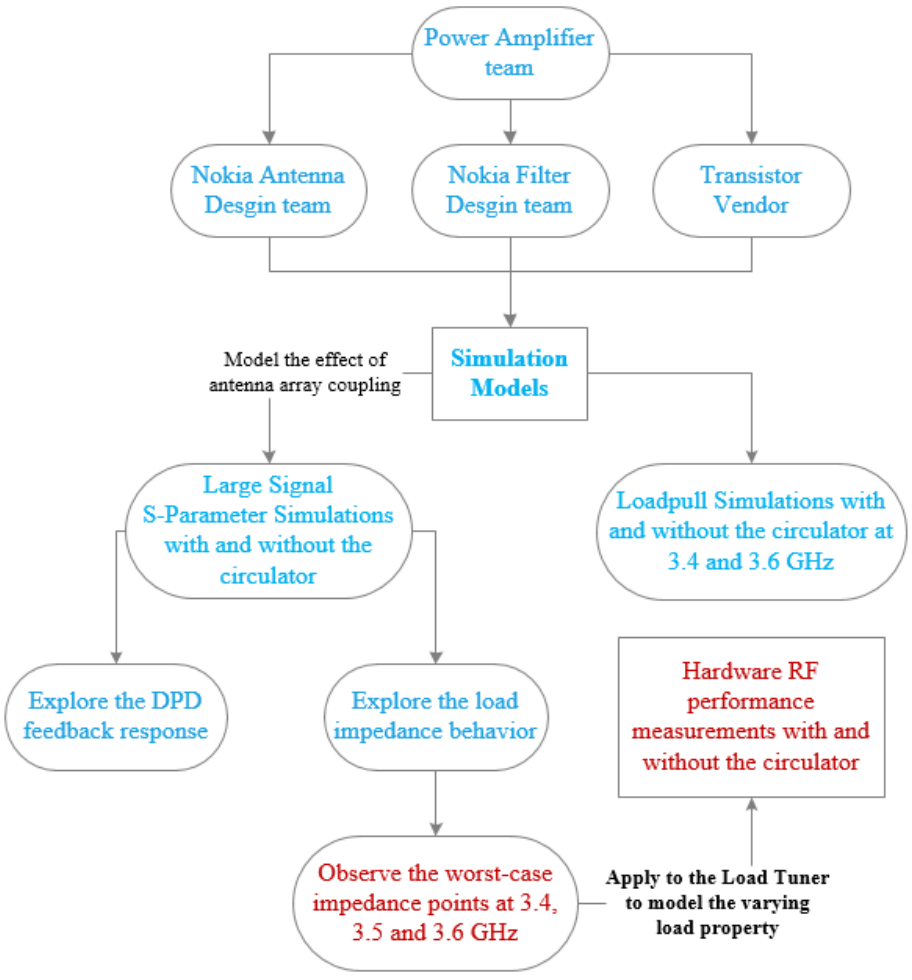

Figure 27 Implementation workflow.

6.4. Simulations

Simulations were performed with simulation models provided by antenna team, filter team and component vendors. The ultimate goal of simulations was to model the worst-case scenario that probably takes place during the transmitting, in which the neighboring TX branches are transmitting with a higher power compared to one which is under evaluation. Then the tapering functionality is modelled but, on the other hand, simulation does not consider the beam steering functionality itself as the antenna simulation model is passive and modelled with certain configuration only. Antenna team provided the simulation model in which the beam steering angle is zero, and therefore the worst-case input impedance condition will most probably not be achieved. But it is still real and sufficient model for modelling the coupling effect. The model includes only four neighboring antenna elements from where the highest coupling action is detected. Ampleon provided the S-parameter data for small signal response simulations and load pull data for transistor level performance evaluation including the output matching circuitry. Thus, simulations are divided into two separate cases.

6.4.1. Large signal S-parameter simulation

To model the antenna coupling, large signal S-parameter simulation configuration was used to add the effect of power difference between TX branches to the simulation. Then the output impedance and DPD feedback response were observed with and without the circulator while the output power in the neighboring branches was swept until the level of 9 dBm higher compared to the branch under evaluation. Large signal S-parameter simulation test bench can be seen in Appendix 1.

The reflection coefficient was measured from the output of the balanced PA structure towards the load provided by either the circulator or the filter. The observation point was determined after the directional coupler which is used for generating the DPD FB response. The load impedance variation between two simulation configurations is modeled in the Figure 28. From there, it is obvious that circulator provides a much more appropriate load conditions over the whole bandwidth compared to case where circulator is removed. Load impedance which is seen without the circulator, provided then by the filter and antenna combination, varies a lot more compared to correspondent measurement points where the circulator exists. Specific load impedance values over the bandwidth are visible in markers.

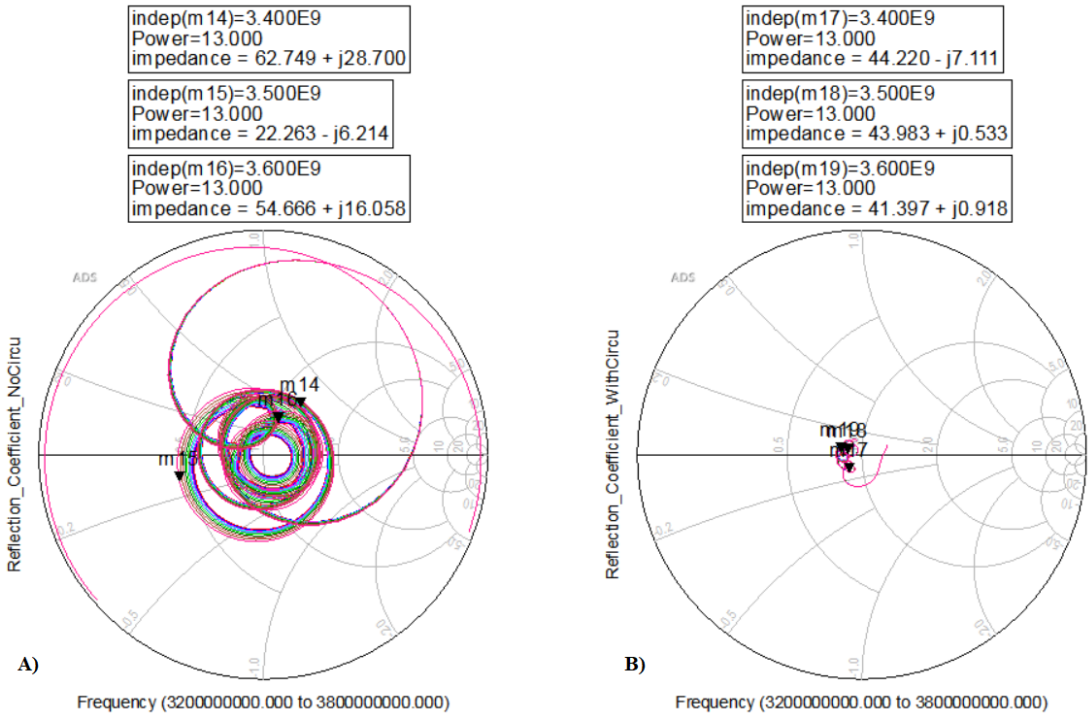

Figure 28 A) Load impedance conditions without a circulator and B) with a circulator. Measured from the output of the balanced PA structure after the directional coupler towards the load.

The effect of higher excitation level in neighboring antenna elements, specifically of them to couple to the element under evaluation, is clearly seen as a noticeable change in input return loss condition, which is modelled in Figure 29. Circulator maintains a proper input return loss value of approximately -20 dB while the antenna coupling highly deteriorates the input return loss values up to levels of -10 dB. However, one should remember that the antenna model used in this thesis does not include any beam steering functionality, which also affects on the input return loss conditions as explained in section 3.3.

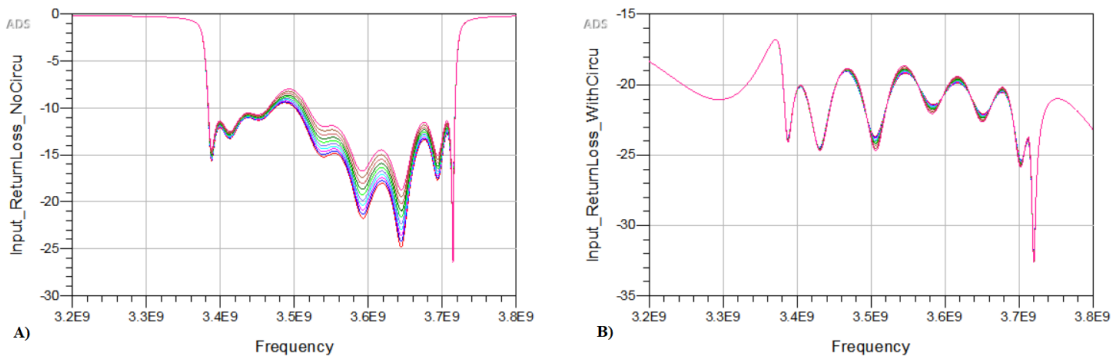

Figure 29 A) Input return loss conditions without circulator and B) with circulator.

There is clear distortion seen regarding the quality of feedback response to digital pre-distorter as seen in Figure 30. A response without circulator differs quite a lot from the one with circulator, which in turn refers well to reference response where the ideal 50Ω load is used. However, according to this simulation result, the amount of the ripple in the feedback response is just meeting the specification which is presented in chapter 6.2.

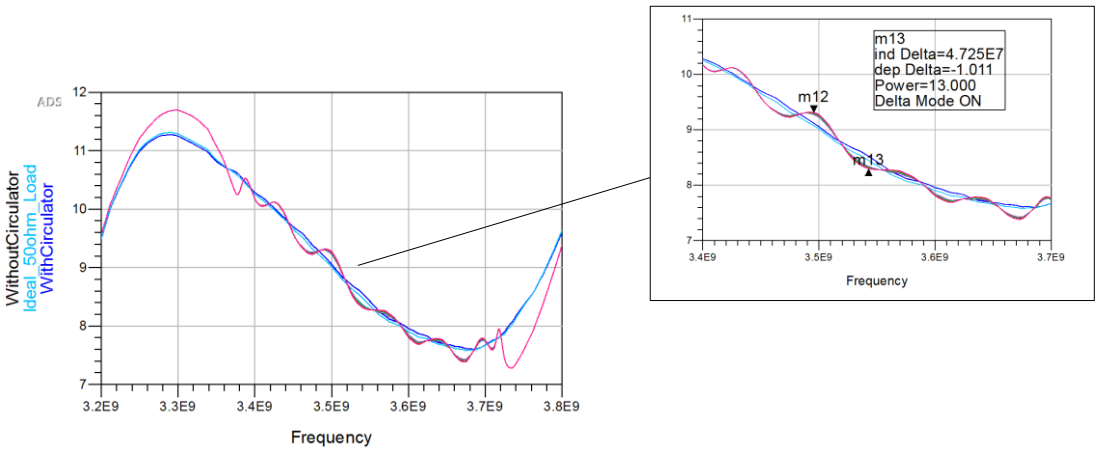

Figure 30 Feedback response to digital pre-distorter.

6.4.2. Load-pull simulations

Load-pull simulations were performed to analyze the PA performance under varying load conditions. Ampleon provided the load-pull model which had been load-pull measured at the 3.4 GHz and 3.6 GHz frequency, and PA performance simulations were again observed with and without the circulator. However, there exists quite a huge limitation regarding the load-pull measurements concerning the configuration used in this thesis, and it is the inability to simulate the balanced structure as the data is load-pulled from the drain lead of the transistor. Therefore, the performance is analyzed only with a single ended structure here and the load-pull test bench can be seen in Appendix 2. Another limitation with load-pull simulation in the scope of this thesis is the inability to simulate specifically at 3.5 GHz frequency, where the worst load condition was found according the Figure 29. Therefore, in terms of RF performance, the worst-case scenario simulation results without the circulator might be even worse from the ones presented here.

Similarly to large signal S-parameter simulations, neighboring branches are having higher power level thus modelling the tapering functionality and affecting most on the antenna input matching conditions of the branch under evaluation as seen in Figure 29. Especially following PA performance properties were examined: efficiency, amplitude conversions (AM-AM, AM-PM), gain and peak power capability. The measurements were also performed against the ideal 50 Ω load as a reference to visualize the ideal transistor level performance compared to load points seen in Figure 28. Load-pull simulation results are compiled in the following table, and they are then explained in more detail.

Table 1 PA performance according to Load-pull simulations

	50Ω Load		**Load with circulator**		**Load without circulator**	
	3.4 GHz	3.6 GHz	3.4 GHz	3.6 GHz	3.4 GHz	3.6 GHz
Max Gain [dB]	36.15	36.01	36.62	35.81	34.95	36.08
Peak power (@3 dB compression) [dBm]	45.4	44.97	45.12	45.02	45.23	44.72
AM-PM (@ Peak PWR) [deg]	-20.43	-23.91	-21.97	-23.97	-23.61	-25.04
Efficiency (@ Pavg) [%]	45.22	42.92	43.54	41.56	44.56	42.58
Efficiency (@ Peak PWR) [%]	47.22	49.47	44.23	48.57	50.09	49.57

Gain behavior of the single ended structure is presented in Figure 31. The linear amplification region, where the gain remains constant, exists in lower output power levels and after certain output power level main amplifier starts to compress. The peaking amplifier contribution is seen as gain response pull back and proper performance is maintained until higher power levels. All AM-AM responses are pretty much equally shaped but as seen, especially simulation towards the load provided by the filter and antenna (without circulator) differs from others at 3.4 GHz frequency (Solid pink line). Even though its maximum gain lags approximately 2 dB from other correspondent simulation results with different load properties, the peak power capabilities at 3dB compression are practically equivalent with having output power values close to 45 dBm. One should remember that the result of the worst load condition at 3.5 GHz is not available, and the peak power capability there will be explored with physical implementation.

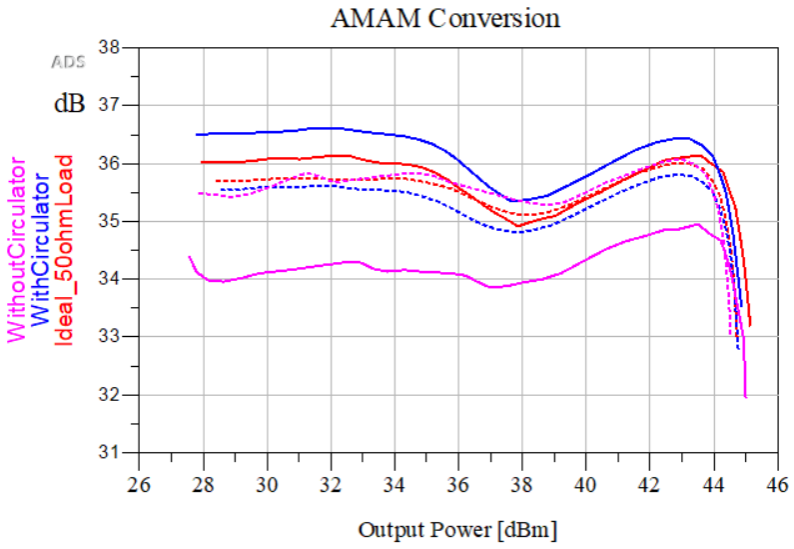

Figure 31 Simulated gain responses with different load conditions (AM-AM). Solid line figures the simulation result obtained with 3.4 GHz frequency and dashed line with 3.6 GHz frequency.

Amplitude to phase conversion response is illustrated in Figure 32. All responses are quite equal with relatively low total phase distortion fulfilling the specification. In DPD point of view, the slope is preferred to be expectable and linear. Therefore, too high response pull-back, which is seen at higher power levels when the peaking amplifier starts to contribute, might be harmful in terms of linearizability, but they are within acceptable limits here. The load without the circulator at the frequency of 3.4 GHz seems to provide the most linear phase distortion response, which most likely correlates to AM-AM conversion figure in terms of main amplifier not compressing that much at the 3.4 GHz.

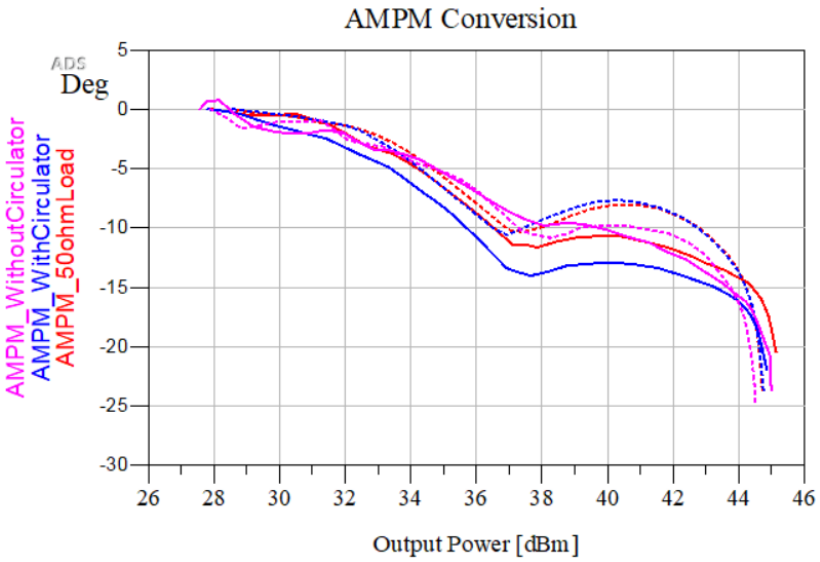

Figure 32 Simulated AMPM responses with different load conditions. Solid line figures the simulation result obtained with 3.4 GHz frequency and dashed line with 3.6 GHz frequency.

Same applies on the efficiency capability too, and the design without circulator provides a bit higher efficiency figures in general compared to one where the circulator is used as seen in Figure 33. Specifically, the best efficiency performance is provided by the circulatorless load at 3.4 GHz frequency. The higher efficiency figures can be explained with lower RF output power requirements when the lossy circulator is being removed: if the same output power level is wanted with the circulator, approximately 0.5 dB higher RF power is needed from the transistor output. This naturally means relatively higher DC current consumption leading to lower efficiency figure according to (5).

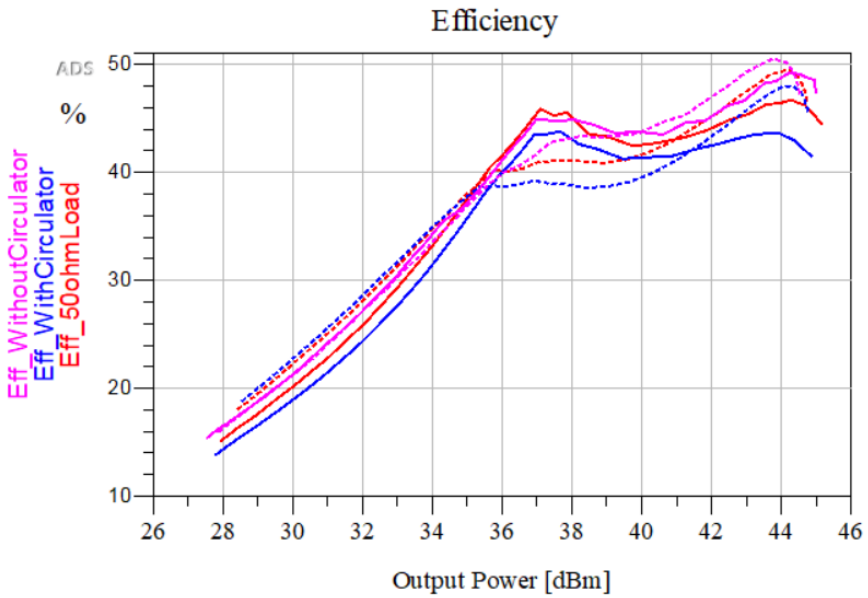

Figure 33 Simulated efficiency responses with different load conditions. Solid line figures the simulation result obtained with 3.4 GHz frequency and dashed line with 3.6 GHz frequency.

6.4.3. Analysis of simulation results

The circulatorless design was investigated in previous chapters with large signal S-parameter and load-pull simulations where the PA performance was compared to the traditional design where the circulator exists and ideal 50 Ohm load. The main interest was to explore the effect of highly changing load which is additionally dependent on the antenna element coupling to the DPD feedback response quality and basic RF performance capability.

Load-pull simulation results are obtained with single ended structure but while the hardware implementation is carried out with balanced structure, ideally the output power and peak power will be increased by 3 dB in the hardware measurements. The balanced structure RF performance is also more forgiving to changing load properties. Moreover, what comes to DPD response quality, the directivity properties of the feedback coupler considerably mitigate the antenna mismatch effect. The reflection coefficient at the antenna input is seen much smaller in the feedback path, since it is multiplied with the directivity value which usually takes small values like 1/10 as explained in [30]. This effect leads to relatively small ripple in the feedback response in Figure 30 even though the real input return loss values at the PA output are varying quite a lot as seen in the Figure 29. According to simulation results, the circulatorless design seems to be feasible as no clear draw-back observed compared to ideal 50 Ω load or to one where circulator existed.

6.5. Physical implementation and hardware measurements

The simulation work was verified with a hardware implementation where the measurements were first performed with a design where the circulator exists and then the layout was modified so that the circulator was bypassed.

The RF performance was noticed to be off the specification and performance expectations after the SMD assembly, so the hardware implementation was started with hands-on tuning. However, in terms of industrial implementation, the difficulty of the integrated Doherty structure appeared here, as the end-user tuning possibilities are quite limited while the main or peak side cannot be tuned separately to meet the RF performance specification. In this design the remaining action was practically bias optimization and output match tuning as the output impedance of the transistor used was 20 Ohm and the matching condition clearly differed a bit from the simulation and demo board implementation. This is most likely due to different relative permittivity (ε_r) valued PCB substrate materials used in demo board and final multilayer structure, and the transformation from the demo implementation to the product board may be inaccurate. The efficiency was managed to get increased by 3% units and the peak power performance by 1dB but they were still lagging from the specification. However, the thesis implementation was carried out with the achieved performance from where the relative change in the performance caused by the changing load properties can be noticed. Hardware implementation measurements are presented in the next section.

6.5.1. Hardware measurements

Hardware measurements were taken at 3.4 GHz, 3.5 GHz and 3.6 GHz frequencies and the corresponding load impedance points, imaging the combined filter-antenna load, were set with a manual load-pull load tuner according the values obtained with large signal S-parameter simulation shown in Figure 28. Hardware measurement results are compiled in the following table, and will be then analyzed in more detail.

Table 2 PA performance according to hardware measurements

		50Ω Load			**Load with circulator**			**Load without circulator**		
		3.4 GHz	3.5 GHz	3.6 GHz	3.4 GHz	3.5 GHz	3.6 GHz	3.4 GHz	3.5 GHz	3.6 GHz
Gain [dB]		31.54	32.69	33.16	31.72	32.25	33.17	30.39	32.55	32.67
Peak power (@3 dB compression) [dBm]		48	47.89	47.5	47.68	47.11	47.02	47.31	48.42	47.09
AM-PM (@ Peak PWR) [deg]		-20.7	-20.5	-14.2	-21.7	-21.5	-18.6	-27.5	-24.3	-16.9
Efficiency (@ Pavg) [%]		32.24	34.28	33.71	30.75	28.49	29.39	27.49	37.31	31.72
ACP	Low	-28.46	-28.36	-29.77	-28.73	-28.62	-30.07	-28.86	-27.95	-30.68
	High	-28.09	-27.61	-29.73	-28.62	-28.51	-29.25	-28.15	-26.75	-30.53

Large signal frequency responses were taken at approximately nominal power conditions, where the antenna load was applied to the PA output to be representing the 3.5 GHz load according to Figure 28. That illustrates the load value where the correspondent antenna element is exposed to dynamically changing input reflection coefficient, as explained in section 3.3, and this load point was chosen as it was supposed to be representing the worst-case scenario. Again, as the load impedance varies over the bandwidth and applied load impedance is valid only in that certain frequency point (here 3.5 GHz), the large signal frequency responses are only indicative on how the worse load property affects compared to ideal 50 Ω load.

From gain response comparison it is seen that worse input return loss condition provided by the antenna cause variation in gain response, and even though the circulator with appropriate isolation properties is used, it does not completely block the effect of reflecting wave.

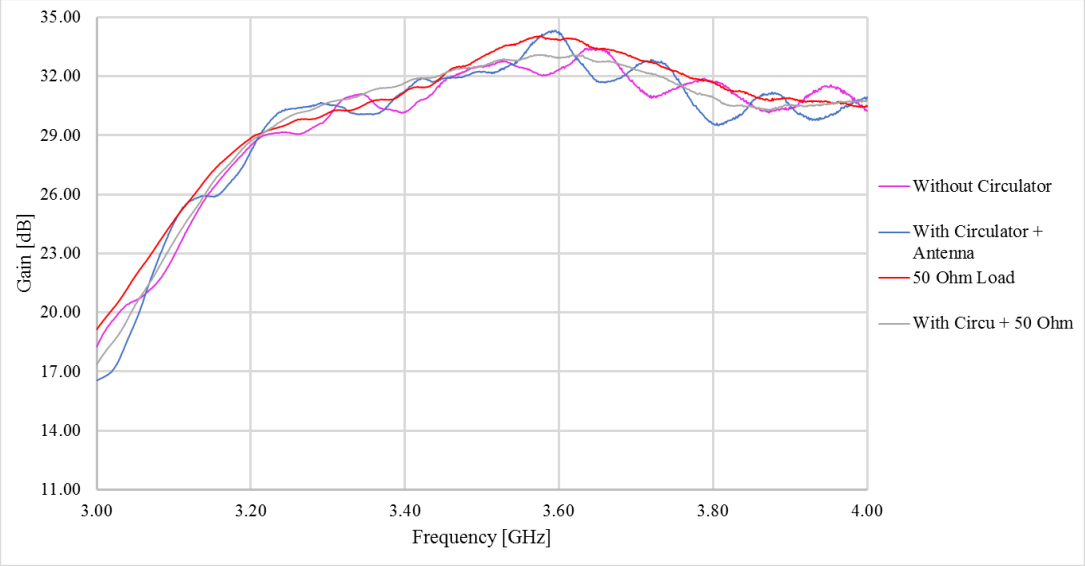

Figure 34 Gain response comparison.

What comes to DPD feedback response quality, the circulator obviously stabilizes the ripple in the response which is caused by the reflective waves as explained in chapter 6.1. The ripple is much higher when the circulator is not used.

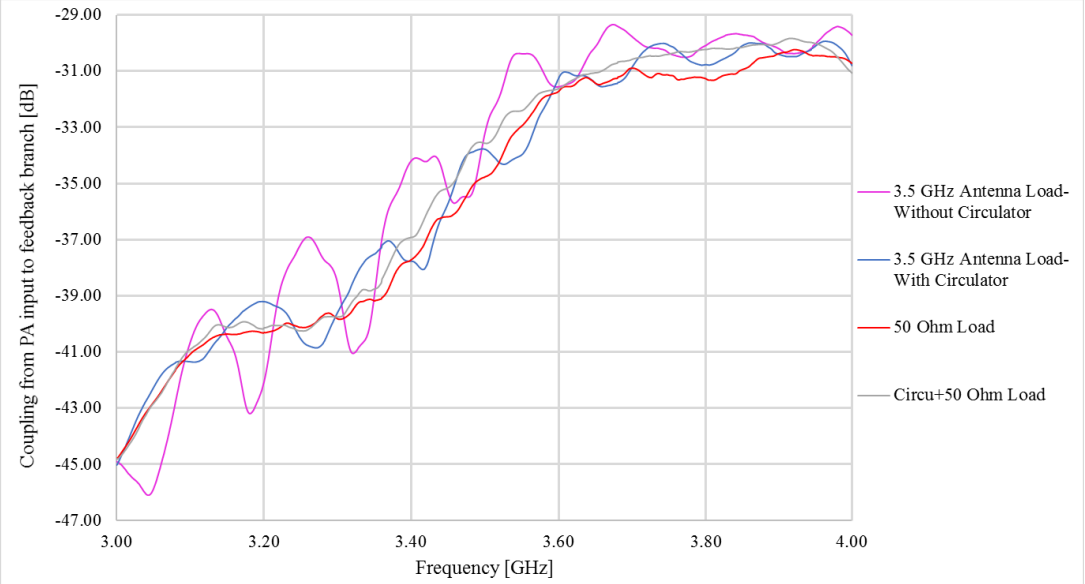

Figure 35 DPD feedback response comparison.

Peak power capabilities were measured with 5 MHz bandwidth 10dB peak to average ratio (PAR) valued LTE signal at 3.4 GHz (Bot), 3.5 GHz (Mid) and 3.6 GHz (Top) frequencies. The AMAM response presented in the Figure 36 was got with ideal 50 Ohm load to use as a reference.

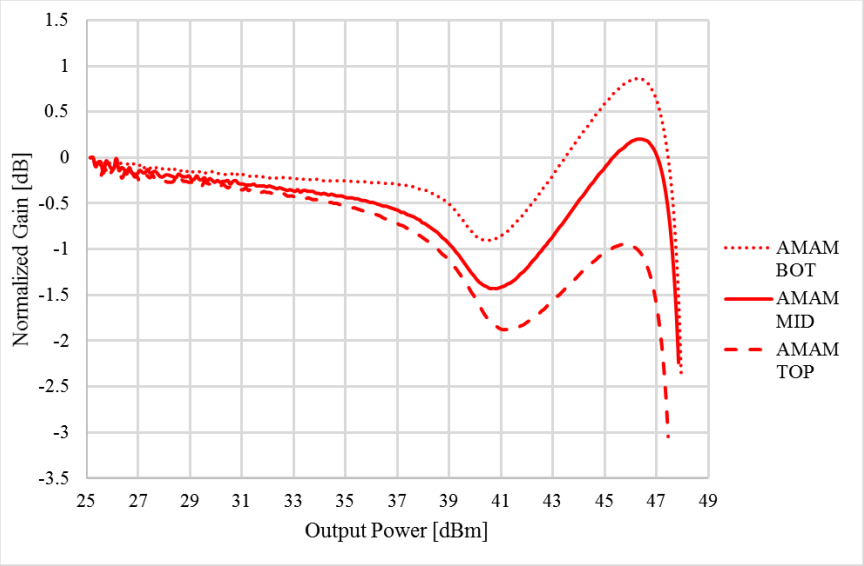

Figure 36 Amplitude conversion measured at 3.4 GHz (Bot), 3.5 GHz (Mid) and 3.6 GHz (Top) frequencies when no circulator was applied and the load was provided by ideal 50 Ohm.

Then, at each frequency point, correspondent load value (*at 3.4 GHz* 62.749+j28.7, *at 3.5 GHz* 22.263-j6.314 and *at 3.6 GHz* 54.66+j16.058) was applied according to Figure 28, and measurements were taken with and without the circulator. When comparing these responses to one obtained with 50 Ohm load, the ultimate peak power capability and the shape of the response seems to remain approximately same. However, peak power capability at the 3.5 GHz without circulator differs clearly form the others. The antenna load with circulator is presented in Figure 37 and without circulator in Figure 38.

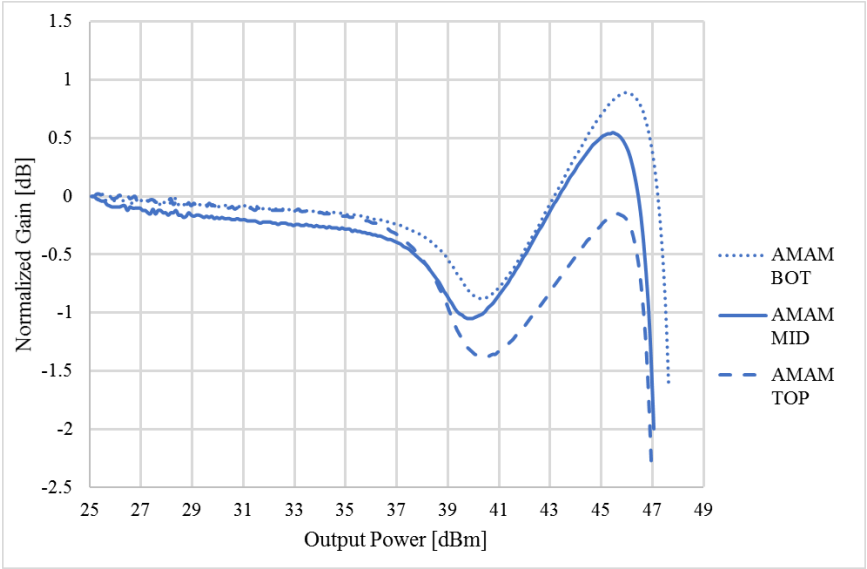

Figure 37 Amplitude conversion measured at 3.4 GHz (Bot), 3.5 GHz (Mid) and 3.6 GHz (Top) frequencies when circulator was applied together with the load provided by the filter+antenna.

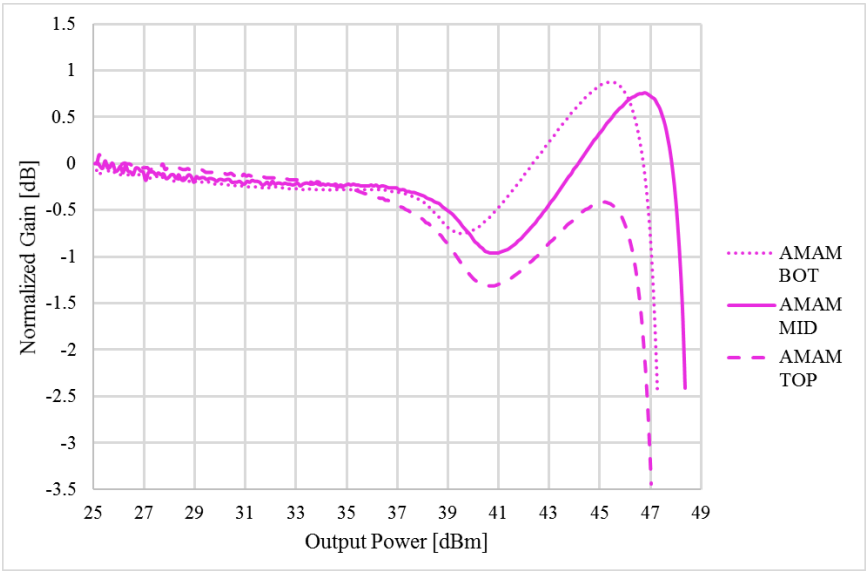

Figure 38 Amplitude conversion measured at 3.4 GHz (Bot), 3.5 GHz (Mid) and 3.6 GHz (Top) frequencies when no circulator was applied and load was provided by the filter+antenna.

When comparing corresponding phase conversion responses, it can be noticed that the shapes are practically equivalent to each other where only slight difference is seen in the response where no circulator was applied. Overall, the absolute phase distortion is approximately same around 20°. Phase conversion responses are presented in following figures.

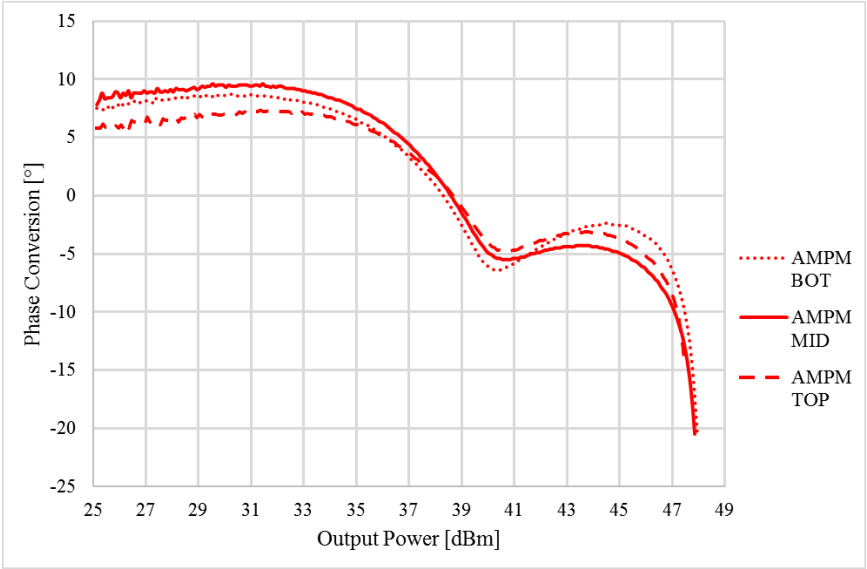

Figure 39 Phase conversion measured at 3.4 GHz (Bot), 3.5 GHz (Mid) and 3.6 GHz (Top) frequencies when no circulator was applied and the load was provided by ideal 50 Ohm.

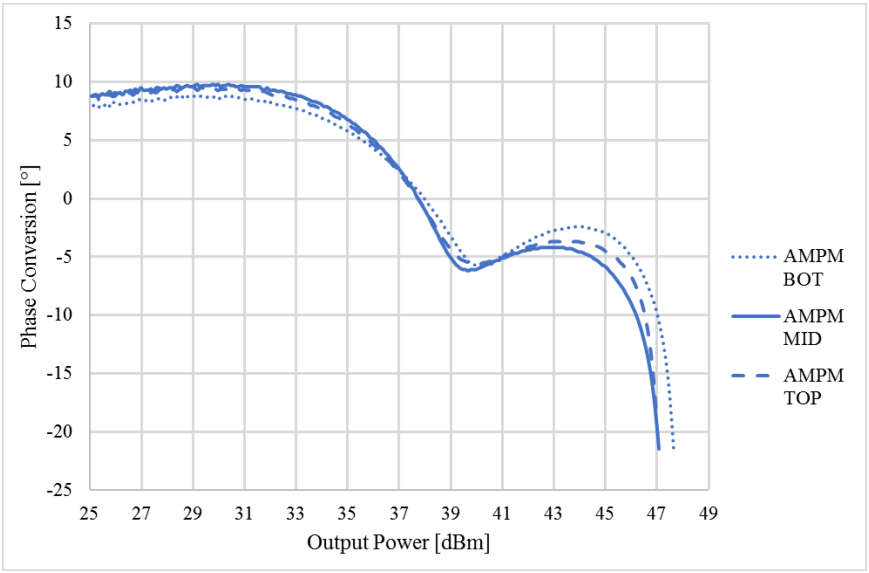

Figure 40 Phase conversion measured at 3.4 GHz (Bot), 3.5 GHz (Mid) and 3.6 GHz (Top) frequencies when circulator was applied together with the load provided by the filter+antenna.

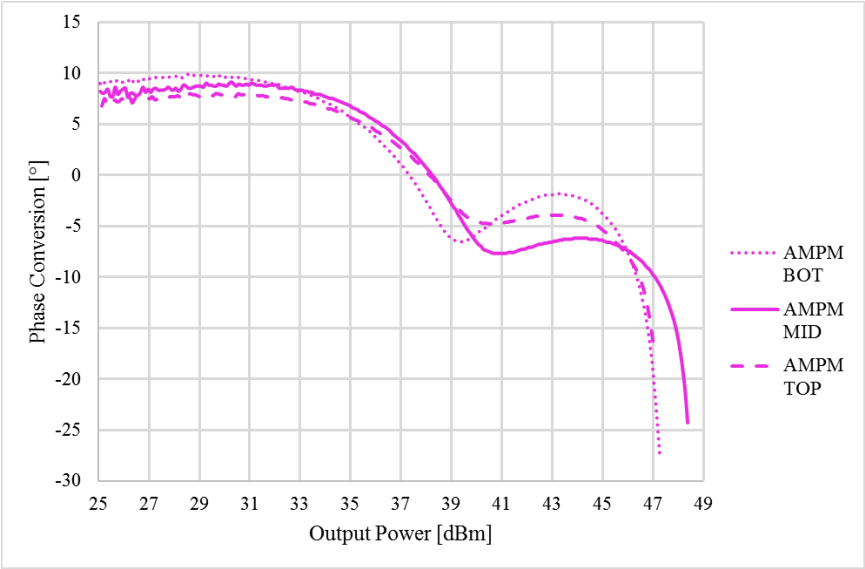

Figure 41 Phase conversion measured at 3.4 GHz (Bot), 3.5 GHz (Mid) and 3.6 GHz (Top) frequencies when no circulator was applied and load was provided by the filter+antenna.

Efficiency figures were measured with 10 MHz bandwidth 6.7 dB PAR valued LTE signal at nominal power conditions at each frequency point together with ACP capability test. Efficiency response over the bandwidth is seen in Figure 42, from where an unexpectable high efficiency capability is noticed at 3.5 GHz frequency in measurement case without circulator.

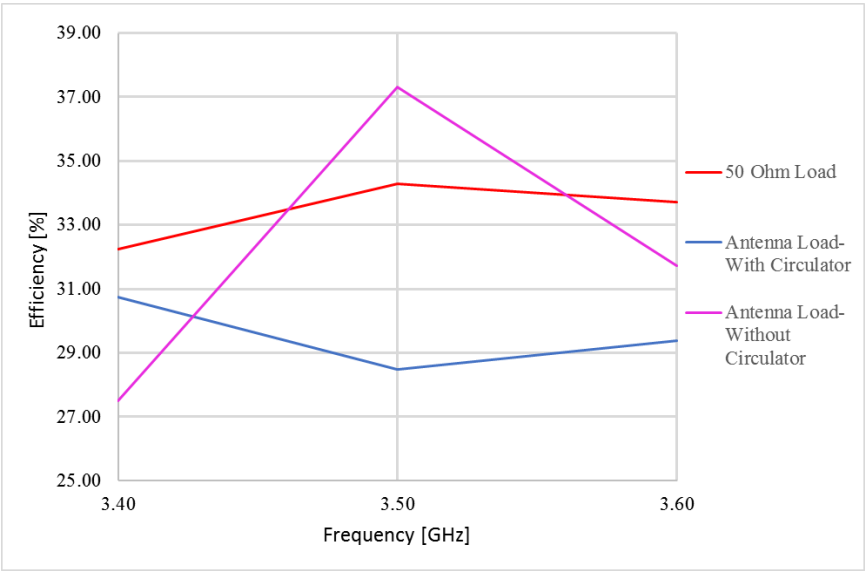

Figure 42 Efficiency over the bandwidth.

6.5.2. Analysis of hardware measurements

There are both pros and cons observed from previously introduced hardware measurement results. Firstly, no noticeable difference is seen neither in amplitude conversion shapes nor the maximum peak power capability at these frequency points but, on the other hand, the ripple in the coupling response at Figure 35 differed a lot compared to simulations presented in Figure 30 and failing clearly from the specification.

One interesting observation compared to simulation results was the significantly higher peak power and efficiency quantities at 3.5 GHz frequency when circulator was not existing. There are two possible explanations for that: in peak power point of view, the 3.5 GHz load (22.263-j6.214) most likely happened to provide complex conjugate match with transistor output matching circuitry for optimum peak power condition. In addition, reverse voltage swing might provide favorable conditions to drain voltage shape thus enhancing efficiency quantity. However, this kind of favorable load condition is not possible to be provided in a real-life implementation because the filter phasing can't be specified and the load impedance is altered to a lot changing property over the bandwidth as seen in the Figure 28.

7. DISCUSSION

While the wireless communication system development is taking fast and major steps towards the 5G technology, general level hardware implementation in the first products is still pretty much similar to previous generations and the R&D work has been pretty much of investigating ways of doing. Complexity of circuit boards has increased a lot in 5G mMIMO units where the amount of TX/RX chains has increased enormously. Therefore, new materials and technologies are being investigated to fulfil for example unit level cooling requirements. However, as is the case in technology development in general, new innovative solutions are needed to be found to keep the achieved market share and earn new ones. The transition to higher frequencies in the hope for wider available bandwidth and increased capacity kind of sets boundaries where certain properties go hand in hand. The fact that propagation capability of higher frequency signals is not that good changes the nature of future base stations in a way where antenna array functionalities take more responsibility of ensuring communication path for every user. Also, the enormous increase in the amount of user equipment force the cell sizes to get smaller, where required transmitting power also decreases compared to older generations. Of course, there is also need for larger cells to add coverage, but they will still be implemented at lower frequencies, e.g. below 1 GHz.

The natural character of higher frequencies enables smaller sized hardware implementations to be feasible because of many hardware properties are relative to the RF frequency, such as $\lambda/4$ impedance transformer in the Doherty topology or ideal antenna array element spacing. The transition to higher frequencies and lower output power requirements have kind of naturally helped transistor vendors to pack more into smaller sized package than before and integrated Doherty structures are now available in the markets. These MMIC (Microwave Monolithic Integrated Circuit) blocks have many helpful characteristics such as internal matching circuitries with even 50Ω in-out properties, auto bias functionalities and multistage configuration. If they are carefully designed with close co-operation between transistor vendor and PA designer, accurate and efficient performance can be achieved to meet customer's needs. Although they have many clear benefits, what would be the case if the performance is found to be off the specification in project phase compared to demo board implementation? Impedance matching network tuning possibilities are zero and project schedules are probably exposed to delays due to fact that transistor vendor then must do the internal design work all over again. There is simply not much to do as a designer in that case which on the contrary is possible at some level when designing traditional higher power Doherty PA structures.

If integration level is increased and more is packed to old space, new unit level challenges are rising such as coupling and cross-talk effects and the unit level cooling arrangement. The total output power of mMIMO base station actually is equal to older generation macro cell base stations (ie.16TX*5W), and circuit boards have to be much more complex to fit all TX/RX chains thus decreasing room from cooling. Therefore, the efficiency of the power amplifier block still remains an important factor even though the output power requirement for each power amplifier has decreased. Also, innovative solutions like embedded thermal coin into the printed circuit board (PCB) must be figured out to get accurate thermal flow from the small sized transistor to the mechanics.

Future technologies are aimed to be cost-effective so transistor level integrations explained above are quite natural in that point of view. Another power amplifier block level solution to improve both cost and space effectiveness could be the removal of circulator, which was investigated in this thesis. The goal was to achieve good understanding of whole unit level operation and to increase the co-operation between teams working close to PA block.

Massive MIMO base station include such a lot functionality and they are more or less complex systems than just different blocks connected together, so efficient early stage system simulation will give huge benefit in accelerating the productization. This so called digitalized R&D necessitates system designers to properly model the site location and the propagation channel properties. Then possible signal blockage effects and blind spots are possible to be noticed, when testing mMIMO implementation with different kind of mMIMO configurations against these real-life conditions.

Smaller scale simulations still include block level verification, and this thesis also begun with simulations. As a result, the importance of proper simulation models and comprehensive simulation work was observed to be essential. The most beneficial situation would be to receive an active model at least from the transistor vendor which could be then integrated to the active antenna model where different kind of beamforming functionalities could be tested through, and power amplifier verified against real world conditions.

This was the first limiting factor in this thesis, as the transistor vendor could only provide small signal and load-pull data based simulation model, and therefore complex nonlinearity effects could not be modelled. Generally, the load-pull data is often sufficient when optimizing Doherty loads in traditional PA design work, but in this work active model would have been essential because of the dynamically changing load property. Also, the antenna model was not modeled under the beam steering functionality (phase difference between the excitation signals of neighboring elements was 0°), so the only real-world case being able to model was tapering functionality, where the power difference between neighboring TX paths and the one under evaluation was being controlled. Passive models only have data from certain use cases, and are thus inadequate compared to active models. For illustrating the coupling effect between adjacent TX branches and its contribution to the input impedance conditions, these models however were sufficient.

Another limiting factor was that even if transistor model would have been more comprehensive covering the whole power and frequency scale, the antenna model would have been designed with different software provider and their integration together would not have been possible. The most optimum situation would be to have active model of at least nonlinear amplifier and functional antenna from same software provider and then simulate the performance against the real load values that correlate to antenna array configuration.

The most time-consuming task in this thesis was to understand the antenna theory and antenna array functionalities properly, and their relation to input impedance conditions, or in the other words, to the load conditions provided to power amplifier output. First there were also difficulties to figure out how the antenna model was modelled and to obtain proper simulation results. Quite many discussion sessions were needed to be held before the understanding between co-operative teams was achieved. After the coupling effect and the contribution of circulator removal to the load impedance was successfully detected, the next challenge was to figure out how to make use of the load-pull data simulation model. One more draw-back occurred there, which

was the inability to model the balanced configuration used in hardware implementation as the load-pull data was measured from the transistor lead. This was not concerned to be major problem though, as the balanced structure used in final the hardware implementation was assumed to behave more forgivingly against the varying load condition compared to a single ended counterpart. Additionally, due to fact that transistor vendor had to change the internal design after the demo phase to fix the stability problem, the simulation model does not match to the final sample which was used in hardware measurements. This was not concerned to be problem either because according to vendor, profound nature of the transistor remained same but the gain was being lowered.

According to simulations, the circulatorless design seemed to be feasible as the removal of the circulator did not affect to the RF performance quantities that much. The variation in efficiency figure was just 2% units from 3.4 GHz to 3.6 GHz in a case where circulator was being removed while it was the same with circulator too, and the peak power varied 0.5 dB vs. 0.1 dB respectively. Also, hardware measurements kind of showed up the potential too, but there occurred a lot more variation in the RF performance figures over the bandwidth, which is not the wanted operation. The variation was large especially in efficiency and peak power quantities. The efficiency variation over the bandwidth (3.4 GHz - 3.5 GHz - 3.6 GHz) was 8.3% units without circulator, while it was 2% units in the design with the circulator. In a similar way, peak power quantities were varying 1.5 dB vs. 0.5 dB. Hardware measurements seemed to be realistic as the better efficiency quantities were also seen as worsened ACP quantities.

On the other hand, no extremely bad performance occurred either in hardware measurements as the worst results without the circulator were on line with the ones where the provided load was having more stable load values. The one thing which should be aware of is the increased ripple in the DPD feedback response which had value of 4 dB according to hardware measurements. This was not expected to be that high as the coupler directivity was assumed to help more in mitigating the effect of worsened reflection coefficient. This rises the need for more complex DPD equalizer and signal modelling, where these coupling effects and reverse voltage swings could be taken to account. One possibility is adaptive gain correction, where estimation and normalization of load mismatch gain is performed, which is presented in [30]. Future work should also include the testing of DPD capability against these varying load conditions whether there is correlation between the distorted feedback response quality and adaptation performance or not.

One should remember that measurements were being taken only in few frequency points so proper analysis against all load properties can't be made, and there might be occurring even bigger variation if the PA could be measured with real functionating antenna. Now load properties are manually set with load tuner according to values obtained with simulation, so going through all values would have required enormous work. Interesting observation was also that the load property which was assumed to be the worst-case scenario (load point at 3.5 GHz frequency: 22.263-j6.214) pointed out to provide the best performance. This has already been discussed in chapter 6.5.2. Another point worth to mention, is that Hardware measurements were performed with 5 MHz and 10 MHz bandwidth valued LTE signals as there were not real 100 MHz bandwidth 5G signals available at a time when measurements were carried out.

The reason for simulation results not showing the similar results to hardware implementation is most likely due to the usage of not comprehensive enough simulation models. As the load-pull model was used instead of an active model, for example capability to analyze drain voltage shape and harmonics load or information of complex nonlinearity effects such as memory effects is not available

Future concepts might include some kind of adaptive impedance matching networks for stabilizing the changing load which are already being used at some level in lower power mobile applications. One example of the successful operation of tuneable matching network using same old DPD algorithm is presented in [31] together with [32]. The challenge is that impedance change requirements are most likely high and tuneable components would need to have low losses and be highly linear to meet spectral purity requirements. The difference also is that they are designed to adapt to changing power conditions than changing load property. That kind of concept might include for example a varactor based adaptive matching or a switch through which stable matching network is connected to either high or low load point of antenna thus enhancing efficiency in lower power levels as well.

Perhaps the most profound thing to understand in terms of this thesis is the fact that the load provided by the combination of filter and antenna is not controllable quantity. Probably the most convenient approach would be to specify boundaries within of the load values should remain, and then accept the caused variation in the RF performance and shape of the DPD feedback response. If the removal of the circulator would be more investigated and tried to implement in the future, the deeper and extremely close co-operation with cross-functional teams and transistor vendor is essential. Few key aspects might include to increase the understanding of coupling effects and other antenna array functionalities and their contribution to load conditions. From PA perspective, load requirements should be also shared to filter and antenna development regarding the DPD correction capability and transistor reverse power endurance for example. Also, extremely deep co-development with DPD engineers would be required.

This work taught that even if the proper initial understanding from the work of cross-functional teams is not owned and simulation models are inadequate, the main thing is to start doing. Try to simulate what is capable to do, and then verify with hardware implementation.

8. SUMMARY

While the integration level in future 5G mMIMO base station structure will be increasing and amount of TX/RX chains is increasing enormously, new solutions are needed to be developed in the power amplifier level too. In this thesis, the goal was to investigate if the removal of lossy component circulator is feasible to achieve the cost and size effectiveness in terms of not deteriorating the power amplifier RF performance too much. The device under test was three stage integrated Doherty transistor, which was connected as a balanced structure. The operation bandwidth was 3.4 GHz-3.6 GHz. In addition to RF performance, considerations were also made on the DPD correction capability point of view.

Thesis started with antenna theory to better understand antenna functionalities and their affect to power amplifier output load properties. Antenna theory was followed by power amplifier theory where basic PA metrics and definitions were introduced together with nonlinear effects and PA topologies. Theory section was then followed by implementation section.

The removal of circulator was first investigated with help of simulation work which was then evaluated with hardware implementation too. Simulation results did not match with hardware measurements, which is most likely due to usage of inadequate simulate model where nonlinear effects are not modelled. There were few other limiting factors concerning simulation work too, but they were not seen as major drawbacks. The investigation was carried out by comparing the performance to the design where circulator was existing. Hardware measurements were performed with 5 MHz and 10 MHz bandwidth valued LTE signals as there were not real 100 MHz bandwidth 5G signals available at a time when measurements were carried out.

Thesis started with simple premise that reflecting signals cause distortion to DPD feedback response, but no thought could be made on the RF performance perspective. Results were promising in that point of view that even though there was more variation in the RF performance when the circulator was removed, extremely bad performance did not occur either. Therefore, a lot more investigations are needed to cover whole frequency band properly and to ensure proper operation in real life use-cases.

9. REFERENCES

[1] Osseiran Afif, Monserrat Jose F., Marsch Patrick (2016) 5G Mobile and Wireless Communications Technology, 410 p.

[2] Nokia Networks, Whitepaper- 5G use cases and requirements, 2016.

[3] Ericsson "Mobile traffic Report Q3 2017" (Read 20.04.2018). https://www.ericsson.com/en/mobility-report/reports/november-2017/mobile-traffic-report-q3-2017.

[4] Ericsson "Mobile subscriptions worldwide outlook" (Read 20.04.2018) https://www.ericsson.com/en/mobility-report/reports/november-2017/mobile-subscriptions-worldwide-outlook.

[5] Lili Wei, Rose Qingyang Hu, Yi Qian, Geng Wu, Key Elements to enable Millimeter Wave communications for 5G wireless systems, IEEE Dec 2014.

[6] Shahid Mumtaz, Jonathan Rodriguez, Linglong Dai (2016) mmWave Massive MIMO: A Paradigm for 5G, Academic Press, 343 p.

[7] GSM Association, 5G Spectrum-Public Policy Position, November 2016.

[8] Ariel Luzzatto (2017) Wireless Transceiver Design: Mastering the Design of Modern Wireless Equipment and Systems. Wiley. 265 p.

[9] Baliga B. Jayant. (2005) Silicon RF Power Mosfets. World Scientific Singapore. 302 p.

[10] Discussions with colleagues.

[11] Constantine A. Balanis. (2005) Antenna theory, Analysis and Design, 3rd edition, Wiley. 1060 p.

[12] Kildal Per-Simon. (2015) Foundations of antenna engineering: A unified approach for line-of-sight and multipath. Artech House Boston. 455 p.

[13] Walker J. (2012) Handbook of RF and Microwave Power Amplifiers. Cambridge University Press, Cambridge. 687p.

[14] Cripps S.C. (2006) RF Power Amplifiers for Wireless Communications, 2nd edition. Artech House Inc., Norwood. 456 p.

[15] Rahkonen T, Vuolevi J, (2003) Distortion in RF power amplifiers, Artech House, 265 p.

[16] Holster J. (2001) RF Power Amplifier Design For A Linearized Transmitter. Master's Thesis. University of Oulu, Department of Electrical Engineering, Oulu.

[17] Peter B. Kenington (2000) High Linearity RF Amplifier Design. Artech House. 531 p.

[18] Marian K. Kazimierczuk (2008) RF power amplifiers. John Wiley & Sons. 405 p.

[19] Vuolevi J., Rahkonen T., Manninen J. (2001) Measurement Technique for Characterizing Memory Effects in RF Power Amplifiers. IEEE Transactions On Microwave Theory and Techniques, Vol. 49, NO. 8.

[20] Franco Sechi, Marina Bujatti, (2009) Solid-state Microwave High-power Amplifiers. Artech House.

[21] Harvala S. (2011) Optimization of the Driver Amplifier in a High-Efficiency Transmitter. Master's Thesis. University of Oulu, Department of Electrical and Information Engineering, Oulu.

[22] John L. B. Walker (2012) Handbook of RF and Microwave Power Amplifiers. Cambridge University Press.

[23] Seyed Aidin Bassam, Mohamed Helaoui, Fadel M. Ghannouchi. (2009) Crossover Digital Predistorter for the Compensation of Crosstalk and Nonlinearity in MIMO transmitters. IEEE Transactions on Microwave Theory And Techniquesm Vol. 57 NO. 5.

[24] Narendra Kumar, Andrei Grebennikov (2015) Distributed power amplifiers for RF and Microwave Communications. Artech House.

[25] S.J.C.H Theeuwen and J.H.Quershi (2012) LDMOS Technology for RF Power Amplifiers. In IEEE Transactions on Microwave Theory and Techniques, May 2012, Vol 60 Issue6, pp. 1755-1763.

[26] Terry Milward (2005), Biasing LDMOS FET devices in RF power amplifiers. Elektron November 2005.

[27] Andrei Grebennikov, Narendra Kumar, Binboga S. Yarmanm (2016) Broadband RF and Microwave Amplifiers. Taylor & Francis Group.

[28] Kaikkonen J. (2016) Asymmetrisen Doherty-vahvistimen suunnittelu RF-Tehovahvistimen pääteasteeksi. Master's Thesis. University of Oulu, Department of Electrical Engineering.

[29] Barradas, Gomes, Cabral. (2017) Power, Linearity, and Efficiency Prediction for MIMO Arrays with Antenna Coupling. IEEE 2017.

[30] Amadou Mbaye (2013) Effect and adaptive correction of impedance mismatch between the antenna and power amplifier on the digital predistortion, 2013.

[31] César Sánchez-Pérez, Jesús de Mingo, Paloma Garcia-Dúcar, Pedro L. Carro, Antonio Valdovinos. (2010) “Optimization of the Efficiency and Linearity in RF Power Amplifiers under Load Variations using a Reconfigurable Matching Network” IEEE 2010.

[32] César Sánchez-Pérez, Jesús de Mingo, Paloma Garcia-Dúcar, Pedro L. Carro, Antonio Valdovinos, (2011) “Improving Digital Predistortion Mismatch Sensitivity using Tunable Matching Networks” IEEE 2011.

10. APPENDICES

Appendix 1. Large signal S-parameter test bench
Appendix 2. Load-Pull data test bench for evaluating the transistor performance

Appendix 1. Large signal S-parameter test bench (Cutted part is similar to one in the middle)

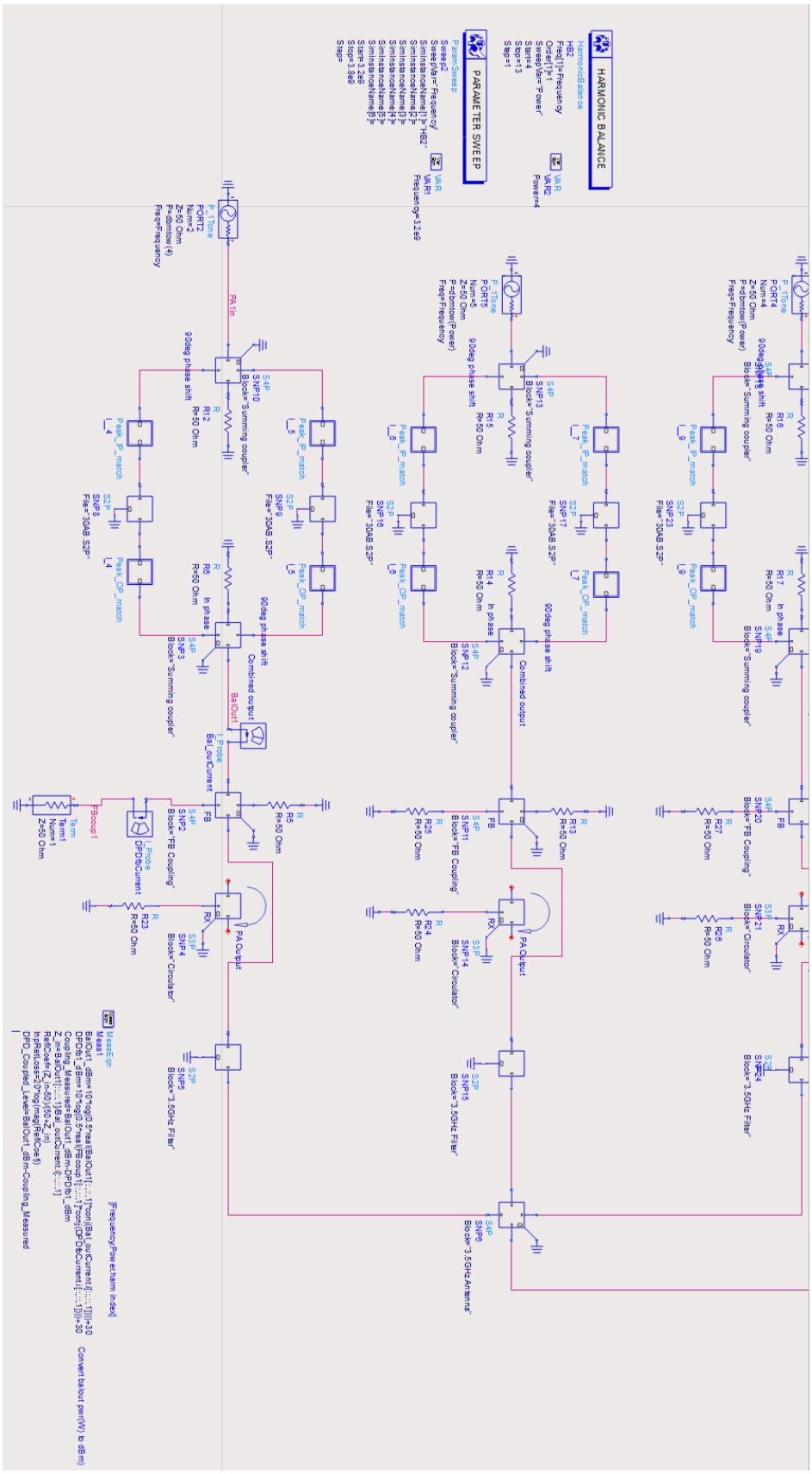

Appendix 2. Load-Pull data test bench for evaluating the transistor performance. (Cutted part is similar to one in the middle)